THEMATIC ISSUE

LA-ICP-MS analysis of trace and rare-earth element distribution in calcite fracture fillings from Forsmark, Simpevarp and Laxemar (Sweden)

Annemie Kusturica[1] · Neele van Laaten[1] · Henrik Drake[2] · Thorsten Schäfer[1]

Abstract

Concentrations and spatial distribution of trace elements in secondary minerals provide valuable information about mobility controlling processes in natural fractures. Important examples include rare-earth element contents that act as analogues for the retention of trivalent actinides such as Am/Cm or Pu(III). The secondary phases (carbonates) investigated in this study originate from exploration drilling bore cores of the Swedish Nuclear Fuel and Waste Management Company SKB (Forsmark, Simpevarp and Laxemar, Sweden).

Here, high-resolution element analysis (Micro-X-ray Fluorescence-Spectrometry (µXRF) and Laser Ablation-Inductively Coupled Plasma-Mass Spectrometry (LA-ICP-MS)) is applied to scan for Na and the trace elements Mn, Fe, Sr, Pb, Th and U as well as the rare-earth elements Y, La, Ce and Yb associated with carbonate fracture fillings. High resolution element maps highlight growth zones and microstructures within the samples, which are not detected by the usual point and line measurements. Evidence of phase-dependent partitioning is observed.

The partition coefficients, *D,* determined from formation water and carbonate data were compared to experimentally generated coefficients and values derived from a 17-year precipitation experiment carried out at the Äspö Hard Rock Laboratory (HRL). Distribution coefficients of the light rare-earth elements La and Ce have been found to be relatively high in the studied samples, whereas the coefficients of distribution of Sr and U are remarkably low.

Overall, the results of this work show that the secondary calcite formed in deep granitic fractures coprecipitated periodically with significant amounts of radionuclide analogues (i.e., rare-earth elements).

Keywords LA-ICP-MS · Calcite · Trace element · Rare-earth element · Partitioning coefficient

✉ Annemie Kusturica
annemie.kusturica@uni-jena.de

1   Applied Geology, Institute of Geosciences, Friedrich Schiller University Jena, Burgweg 11, 07749 Jena, Germany

2   Department of Biology and Environmental Science, Linnaeus University, 39182 Kalmar, Sweden

Introduction

Ever since nuclear power plants have been part of the civil energy mix, the responsible long-term disposal of the radioactive waste and isolation from the biosphere has been a major challenge. Even though radiotoxicity gradually declines over geological time (Joyce 2017), the long persistence of nuclear waste and its decay products require a carefully selected concept for the long-term storage (Ojovan et al. 2019). Crystalline rocks are widely discussed as one suitable host rock formation for the deep geological disposal of spent nuclear fuel (SNF). To this day, major investigation campaigns on crystalline host rock are carried out for example at the Fennoscandian Shield of Sweden and Finland (Andersson et al. 2013; Milnes et al. 2008), at Archean granite-gneisses in Siberia (Laverov et al. 2016), or within underground research laboratories such as the Grimsel Test

Site (GTS, Switzerland, Quinto et al. 2017) and the Korean Underground Research Tunnel (KURT, Korea) (Kwon et al. 2006). These site investigations contributed to the profound understanding of retention and transport mechanisms in the context of SNF disposal. In this context, fracture-fillings are of special interest as they are expected to control radio-nuclide (RN) mobility by sorption and/or incorporation through solid solutions (OECD/NEA 2007).

Since the experimental verification of man-made RN retention in fracture fillings through geological time scales is not feasible, natural analogues like rare-earth elements (REE) and their incorporation have been used in a well-founded approach (Eisenbud et al. 1984; Johannesson et al. 1995; Smellie and Karlsson 1999; Dobashi and Shikazono 2008).

Due to their similar chemical behavior (i.e., $5p^66s^2$ configuration of the outermost atomic shell, lanthanoid and actinoid contraction, mostly trivalent state under natural conditions) REE can serve as natural analogue to estimate the fate and mobility of actinides such as Pu(III), Am(III) and Cm(III) (Krauskopf 1986; Bruno and Sandino 1987; Zhong and Mucci 1995). Bruno and Sandino 1987 furthermore described the use of Th as analogue for tetravalent actinides (Pa(IV), U(IV), Np(IV), Pu(IV)).

This study focuses on the fracture filling carbonates from granitoid host rocks in Forsmark, Simpevarp and Laxemar, Sweden. Forsmark is the planned spent fuel repository site, whereas Simpevarp and Laxemar have been intensely studied in the siting process as one candidate area by Svensk Kärnbränslehantering; SKB (Hedin 2006).

Trace element (TE) incorporation in carbonate fracture fillings is highly sensitive to changes of the precipitation environment, e.g., pH value, oxidation state, TE speciation, temperature, salinity, precipitation rate, pressure and characteristics of the precipitation solution, e.g., aqueous TE/Ca ratio, adsorption–desorption equilibrium of TE at the crystal surface and microbial activity (Lorens 1981; Zhong and Mucci 1989; Rouff et al. 2005; Tang et al. 2008; Day and Henderson 2013; Füger et al. 2019; Smrzka et al. 2019). Hence, the study of the spatial trace element distribution within the fracture filling minerals can help to reconstruct the paleo-hydrogeological evolution of the site (Tullborg et al. 2008; Milodowski et al. 2018; Mizuno et al. 2022). In the context of SNF storage, these findings allow us to estimate the potential TE retention under prospective hydrogeologic and climatic changes.

At Forsmark, Simpevarp and Laxemar the fracture systemof the granitoid bedrock is filled with assemblages of hydrothermal, sedimentary and low temperature fracture fillings formed at intermittent fluid flow events. Low temperature carbonates in Forsmark, Simpevarp and Laxemar show enrichments in REE and other elements, e.g., Mg, Mn, Fe, Sr, Th and U (Landström and Tullborg 1995; Drake et al.

2012, 2018; Maskenskaya et al. 2015). TE analyses of these fracture coatings have been carried out mainly on ground and dispersed bulk samples or as point measurements on intact rocks.

In contrast to previous works, this study aims to gain a more detailed understanding of the structural incorporation of TEs in calcite fracture-fill. High-resolution spatial distributions allow for a precise evaluation of the formation conditions and their influence on element retention. In this study, µXRF and LA-ICP-MS were used to examine the distribution patterns of the trivalent REEY, especially Y, La, Ce and Yb in association with other common elements (Na, Fe, Mn, Sr, Pb, Th, U). Comparing calcite compositions and groundwater compositions from the same (or adjacent) borehole sections enable calculation of apparent TE/Ca partitioning coefficients, which signify the role of solid solutions in the mobility of RN under natural conditions. Based on these results, precipitation rate and plausibility of the interpretations were estimated.

Geology

Simpevarp and Laxemar site is located ca. 320 km southof Stockholm at the Swedish east coast (Fig. 1). The nuclear power plant of Oskarshamn and the Äspö Hard Rock Laboratory (HRL) are in close proximity to the site. The Forsmark site is located ca. 350 km to the north of Oskarshamn, adjacent to the Forsmark nuclear power plant (Fig. 1). The sites are situated in the Svecokarelian Orogen of the Fennoscandian Shield. The predominantly igneous bedrock (ca. 1.91–1.75 Ga) underwent numerous cycles of mostly Proterozoic tectonic deformation and magma intrusions and was uplifted later in time (Guenthner et al. 2017). The sites belong to different tectonic units and were affected by early ductile and later brittle deformation, i.e., Sveconorwegian faulting, late- and post-Caledonian faulting, and Permian extension (Hermansson et al. 2007; Viola 2008; Viola et al. 2009; Saintot et al. 2011; Tillberg et al. 2020, 2021). Simpevarp and Laxemar belong to the Transscandinavian Igneous Belt (TIB) which was formed ca. 1.85–1.66 Ga ago (Högdahl et al. 2004) in the context of the volcanic activity related to the subduction alongside the Svecokarelian orogeny, to which Forsmark belongs (Wahlgren 2010). The TIB consists of granite to quartz monzodiorite to diorite gabbros. These areas experienced further major periods of igneous activity viz. the granitic magmatism ca. 1.45 Ga ago linked to the Hallandian orogeny and the intrusion of dolerite dykes (ca. 0.9 Ga) in the TIB due to the Sveconorwegian orogeny (Söderlund et al. 2005; Wahlgren et al. 2007). The long-term uplift of the region enabled the manifestation of a sub-Cambrian unconformity followed by several cycles of loading and unloading. Present regoliths are assumed to be

Fig. 1 Map of the study sites Simpevarp, Laxemar and Forsmark
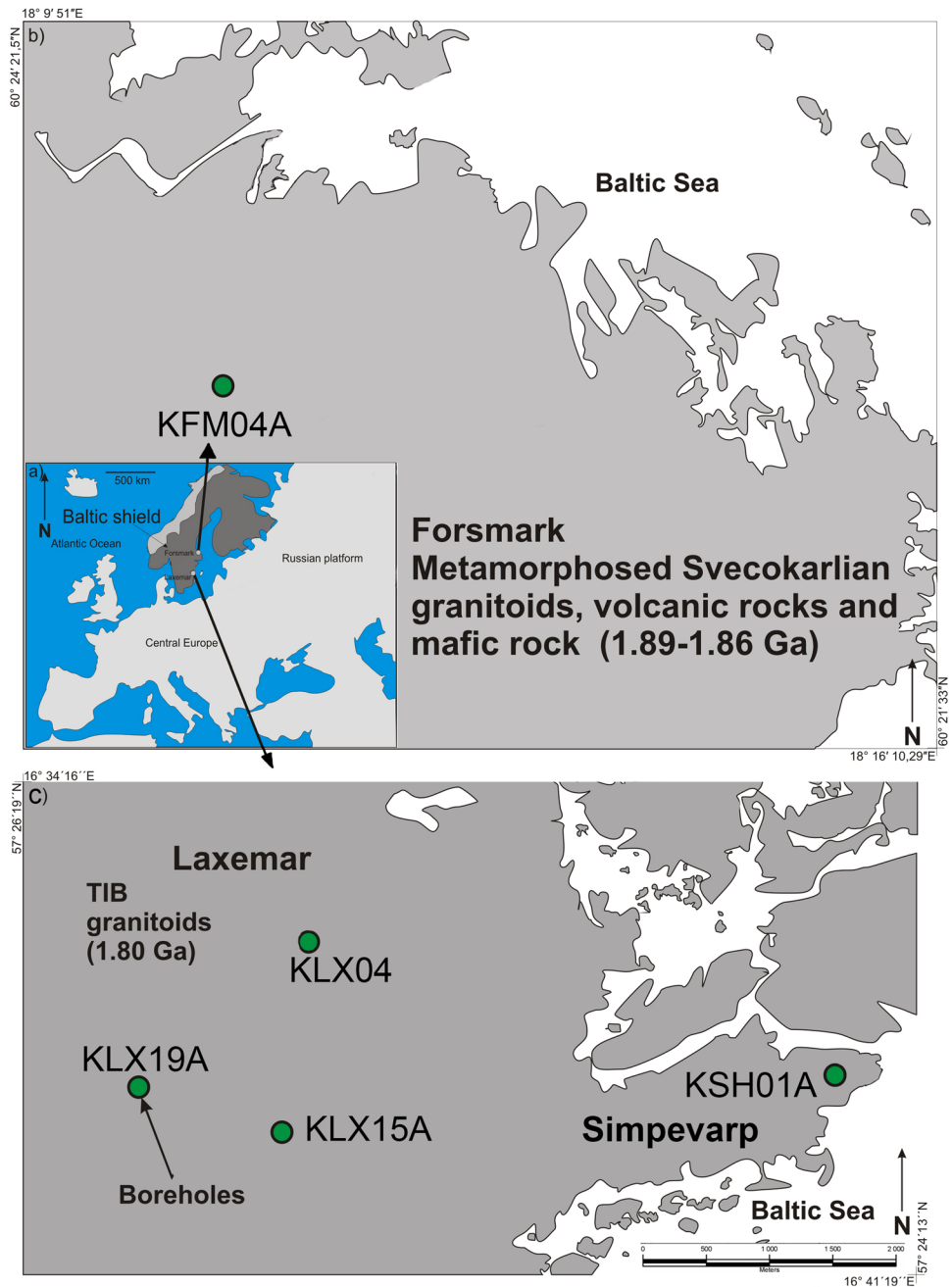
deposited by the end of the last glaciation and after deglaciation (Lundin et al. 2004; Tröjbom and Söderbäck 2006; SKB 2008; Nyman et al. 2008; Brydsten and Strömgren 2010).

During the Quaternary, periods of glaciation, glacial reboundand shoreline displacements shaped the area. Along with the glacial waters, a range of meteoric, lacustrine, brackish, marine, and fresh water, so called end members, infiltrated into deeper aquifers. The paleo-hydrogeological setting has been influenced by the mixing processes of these end members with deep saline waters (Laaksoharju 2004; Laaksoharju et al. 2008a, 2008c; Gómez et al. 2014).

As a result of the complex groundwater evolution in combination with upwelling hydrothermal fluids multiple generations of fracture fillings developed. At both sites, a set of hydrothermal fracture fillings is followed by two younger generations of fracture fillings of low-temperature groundwater precipitates (Generation 3/4 in Forsmark, generation 5/6 in Simpevarp and Laxemar). In this study, low temperature carbonates were investigated (see e.g., Drake et al. 2006, 2009b; Sandström et al. 2008 for detailedoverviews of the fracture filling generations).

Methods

Calcite crystal samples were hand-picked from drill cores taken at the SKB test sites Simpevarp, Laxemar and Forsmark and named according to borehole number and depth in meter (Table 1). Formationwater samples were taken from the nearest possible sampling location in the same borehole (Table 1). The hydrogeochemical data of the formation water samples were provided by the SKB (Table 2) (Laaksoharju et al. 2008b, 2009).

Calcite samples of < 3 cm length were impregnated in Araldite 2020 epoxy resin (Huntsman Corporation, Salt Lake City, Utah, USA) and polished to create a planar surface. For characterization via *Polarized Transmitted Light Microscopy (PTLM)*, thin sections were polished to a thickness of 30 µm. Images were generated using the VHX-6000 Keyence digital microscope (Keyence Corporation, Osaka, Japan) and the research microscope Zeiss Axioplan 2 (Carl Zeiss AG, Oberkochen, Germany).

Micro-X-ray Fluorescence-Spectrometry (µXRF) (M4 TORNADO PLUS µXRF, Bruker Corporation, Billerica, Massachusetts, USA) was used to generate spatially resolved element map scans of the planar sample surfaces. Map scans were measured in one cycle with overlapping spots (spot size 20 µm, spot distance 10 µm) under vacuum condition (20 mbar). The acceleration voltage was 40 keV at 130,000 cps, the time per pixel 15 ms and the energy deviation between 0.4–0.8 meV. Samples with well-distinguished zonation were selected for further analysis.

Laser Ablation-Inductively Coupled Plasma-Mass Spectrometry (LA-ICP-MS) analysis were carried out with a LSX-213 C2 + Laser Ablation System (Teledyne

Table 1 Overview on samples with according research site, bore hole number, depth and prepared section and origin of the associated formation water

Site	Boreholes	At borehole length [m]	Wall rock	Formation water sampling
Forsmark	KFM04A	233	Granitic gneiss	Same section
Simpevarp	KSH01A	205	Fine-grained diorite	Same section
		212		
Laxemar	KLX04	669	Granite to quartz monzodiorite, generally porphyritic	150 m shallower
	KLX19A	414	Quartz monzonite to monzo-diorite, equigranular to weakly	100 m shallower
		428	porphyritic	100 m shallower

Table 2 Hydrogeochemical data of formation water samples from drillings KFM04A in Forsmark, KSH01A in Simpevarp and KLX04, KLX15A and KLX19A in Laxemar, Sweden

Site	Forsmark	Simpevarp		Laxemar		
Bore hole	KFM04A	KSH01A		KLX04	KLX15A	KLX19A
Elevation SecMid (m)	− 199.83	− 243.59	− 150–200	− 486.52	− 467.22	− 413.86
pH (field)	6.74	n.a	n.a	n.a	n.a	n.a
pH (lab)	7.19	n.a	7.24*	7.83	n.a	8.22
Na (mg/l)	1910	2610	1610*	691	2080	962
Ca (mg/l)	1480	1220	692*	234	1540	152
Fe (mg/l)	1.99	0.611	n.a	0.09	0.537	0.0707
Fe_{TOT} (mg/l)	2.13	0.604	1.6*	0.104	0.556	0.084
Fe^{2+} (mg/l)	2.15	0.584	n.a	0.082	0.548	0.074
Mn (mg/l)	3.15	0.626	0.72*	0.109	0.549	0.068
Sr (mg/l)	15.5	21.3	0.72*	4.67	27.7	2.65
Y (µg/l)	1.42	0.422	n.a	0.0877	0.397	0.0533
La (µg/l)	0.296	0.137	n.a	0.139	< LOD	0.0225
Ce (µg/l)	0.315	0.0966	n.a	0.175	< LOD	0.0266
Yb (µg/l)	< LOD	< LOD	n.a	< LOD	< LOD	< LOD
U (µg/l)	27.8	0.074	n.a	0.253	0.144	0.0806
Th (µg/l)	< LOD	< LOD	n.a	0.356	< LOD	< LOD

The samples were taken in close proximity to the fracture fillings listed in Table 2. * Additional groundwater data from (Laaksoharju 2004) were added for drilling KSH01A Section 150–200 m

n.a. no data available, < LOD data below limit of detection

Technologies Inc., Thousand Oaks, California, USA) and XSeries 2 Quadrupole ICP-MS (Thermo Fisher Scientific Inc., Waltham, Massachusetts, USA). For single line scans, a spot size of 30 μm and 80% energy were used, for area scans a spot size of 20 μm and 80% energy were used. Tuning of the ICP-MS was performed using NIST SRM 612 glass standard (National Institute of Standards and Technology, Gaithersburg, Maryland, USA) and USGS MACS-3 was used as an external carbonate calibration standard (United States Geological Survey, Reston, Virginia, USA). Scan Speed was 10 μm/s, energy fluence 10 J/cm^2. Due to the destructive character of the method, direct measurement repetition on the same sample spot is not possible. However, the measurement of the MAC-S 3 standard prior to and after each calcite scan ensured homogeneity and comparability of the measurements. Element specific detection limit (LOD) ranges within one map scan are given exemplarily in the Appendix, Table 9.

The LA-ICP-MS data were processed with the data analysis software Iolite v3 (School of Earth Science, University of Melbourne, Melbourne, Australia) running in IGOR Pro 6 (WaveMetrics Inc., Oregon, USA). Single line scans were hand processed based on a similar approach with Microsoft Excel 2016 (Microsoft Corporation, Washington, USA). Calcium contents were determined by calculating the difference between the stoichiometric values of Ca minus the cumulative trace elements content (Eq. 1):

$$c\left(Ca^{calcite}\right) = 400,400 \; ppm - c(\Sigma TE^{calcite}) \tag{1}$$

Element maps and single line scans allowed the identification of generations of overgrowth. To clearly assign each measurement point of the mappings to a growth zone, multivariate analyses were performed using the software R (version 3.6.1) and RStudio® (version 1.2.5019) with basic packages as well as ggplot2 and psych. Only elements for which a zonation was visible in the element map (Mn, Fe, Sr, Y, La, Ce, Yb, U) were included and the data were log-transformed and auto scaled prior to any multivariate calculations. First, a principal component analysis was performed for each sample. In a next step, only principal components whose scores showed a (spatial) zonation were included in a k-means cluster analysis of the corresponding principal component scores. Different numbers of k were chosen and for each of them the cluster analysis was calculated ten times. The solution to work with was chosen based on a combination of a reasonable number for k (zones not spatially connected should be separate clusters) and the most frequent solution of the ten repetitions.

For single line scans, the contents of the outermost overgrowth were extracted from the hand processed data as the mean of the ten outermost laser spots (100 μm). For map scans, the module *profile points* of the software Iolite was used to extract data points alongside the youngest overgrowth with an estimated thickness of several tens μm.

The REE fractionation was calculated based on the Chondrite normalized La and Yb content of the calcite and the Chondrite normalization factors taken from McDonough and Sun 1995. For sample KSH01A_212, the REE fractionation was evaluated based on Chondrite normalized La/Y ratios as for this sample, no Yb contents were measured.

The partition ratios of trace elements between the formation water and the youngest overgrowth were calculated based on the Henderson-Kracek division coefficient D_{TE} (Eq. 2), (Henderson and Kracek 1927):

$$D_{TE} = \frac{\eta_{TE}^{Calcite} / \eta_{Ca}^{Calcite}}{\eta_{TE}^{Fluid} / \eta_{Ca}^{Fluid}} \tag{2}$$

whereas η is the molar amount of the subscripted element in the superscripted phase.

The precipitation rate R_P was calculated based on Eq. 3 (DePaolo 2011). Experimentally driven TE/Ca partitioning ratios of this work, the equilibrium partition coefficient K_{eq} and the forward partition coefficient K_f taken from DePaolo 2011 and the calcite dissolution rate R_b adapted from (Chou et al. 1989) were applied to Eq. 3:

$$D_{TE} = \frac{K_f}{1 + \frac{R_b}{R_p + R_b}(\frac{K_f}{K_{eq}} - 1)} \tag{3}$$

Results and discussion

Morphology, overgrowth, zonation of the carbonate fracture fillings

Single calcite crystals from Forsmark and Simpevarp show euhedral crystal habitus. The habitus of the single growth zones at the samples KSH01A_205_A/B, that consist of several concentric, accordant growth zones, changes between elongated c-axis (c ≈/> a) and elongated a-axis (c < a).

The sample KFM04A_233 and KSH01A_205_B show inclusions of Fe-oxides/-hydroxides. The sample aliquots of KFM04A_233 and KSH01A_205_A/B consist of single euhedral crystals, whereas the others are healed fracture fillings. The samples KLX04_669 and KLX19A_414/428 display calcite fracture-fill attached to wall rock and display aggregates of anhedral carbonate crystals. Sample KLX04_669 shows traces of wall rock alteration. The fracture wall is rimmed by the oldest generation of euhedral quartz followed by calcite (Fig. 2A andB). Samples from Laxemar (KLX19A_414/428, Fig. 2C and D) show a greenish contact zone (GCZ) within the fracture filling calcite. At

Fig. 2 **A** Polarized transmitted light microscopic image of sample KLX04_669 under parallel polarized light. The white frame marks the detail displayed in picture B. **B** Polarized transmitted light microscopic image of the wall rock/fracture filling contact of sample KLX04_669 under crossed polarized light. The white arrow points at a quartz overgrowth. **C** Image of sample KLX19A_414 with the greenish contact zone. **D** Polarized transmitted light microscopic image of the greenish contact zone at sample KLX19A_428 under crossed polarized light. The black arrow in **C** and **D** marks the greenish contact zone
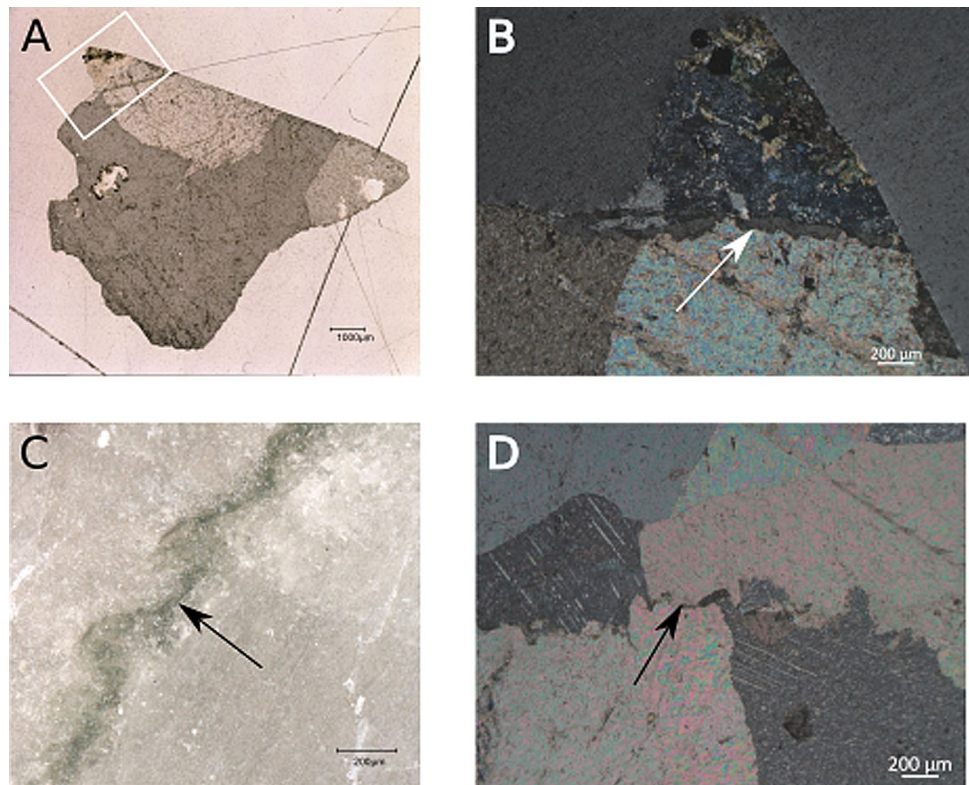
a depth of 414 m, the fracture filling shows anhedral growth with a sudden change of crystal habitus approximately in the center of the fracture (at the GCZ). At 428 m below the surface, the greenish contact zone is expanded to about 3–5 mm with a more symmetrical structure of the growth zones on both sides.

Trace elements composition

Simpevarp

The two samples of the borehole KSH01A, Sect. 205 m, show analogue overgrowths with similar element assemblage but different absolute contents.

At least seven distinct periods of precipitation, with growth zone 1 being the oldest overgrowth, were identified by morphology and trace element assemblage. Based on the qualitative element content, the strictly statistically generated cluster analyses revealed seven and eight clusters shown in Fig. 3. These are, however, not to be confused with the growth zones which were interpreted based on element content, morphology and mineralogy of the fracture fillings. Overall, sample B shows lower TE contents. In both samples, enrichment patterns of light rare-earth elements (LREE) follow the opposite trend as Fe and Mn. At intervals, distribution patterns of Sr are congruent with Mn and Fe. Uranium is strongly enriched in the two youngest growth

zones. Within sample A, similar distribution patterns for Pb, Th and U are apparent. Growth zone 4 of sample A shows signs of face dependent partitioning. The growth zone 5 shows a gradual decline in Na, Mn, Fe, Sr and heavy rare-earth elements (HREE), but increase in LREE. The degree of fractionation of REE differs throughout the samples and reaches highest ratios in zone 2 (median Chondrite normalized ratio: 58.27 for sample A and 5.45 for sample B) and the youngest part of zone 5 (median Chondrite normalized ratio: 236.68 for sample A and 68.79 for sample B). Further similarities are evident for zone 2 and the youngest part of zone 5, e.g., both show strong enrichment in LREE.

The third analyzed sample of borehole KSH01A originates from a depth of 212 m and contains two growth zones. As Yb contents are often below detection limit in this sample, the La/Y ratio is used as indicator of REE fractionation. The older, Fe, Sr and REE enriched zone 1 is subdivided into zone 1a with high TE contents (see Appendix, Figure 9) and zone 1b with decreasing TE contents and REE fractionation in favor of LREE (La/Y ca.1—12.5). Within the adjoined zone 2, TE contents are generally low. The La/Y ratio decline to < 1. The crystal is surrounded by a rim enriched in TEs and REE. La/Y ratios reach values up to > 100.

In general, the observed calcite TE contents are higher compared to sample measurements performed by Drake and Tullborg (2009a), Drake et al. (2012) and Maskenskaya et al. (2015) from comparable depths. Only Th and U contents are
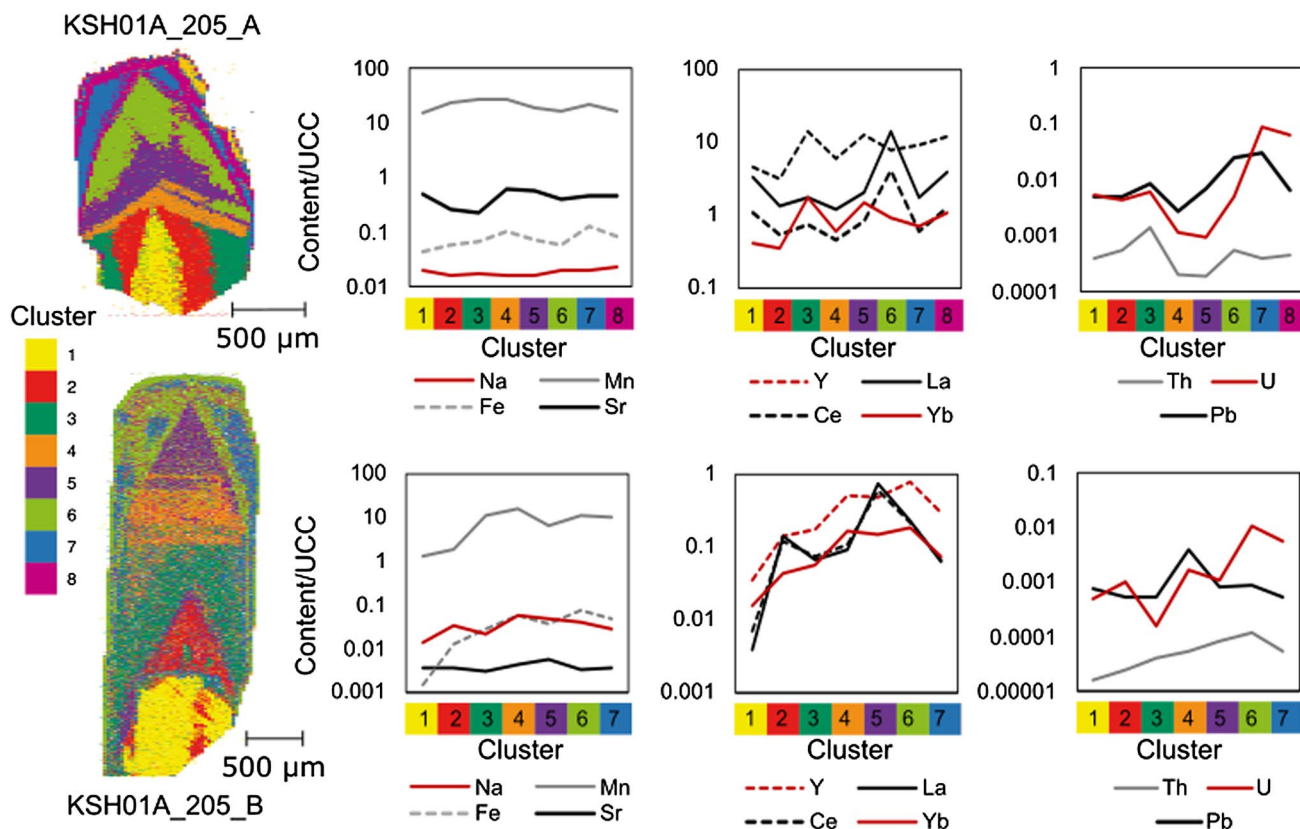
Fig. 3 Trace elements distribution pattern of calcite fracture fillings from bore hole KSH01A (205 m) from Simpevarp. Upper continental crust (UCC) normalized (Wedepohl 1995) mean element contents of sample KSH01A_205_A (**A**) and KSH01A_205_B (**B**) are visualized based on cluster analyses. The clusters are color-coded at the sample maps on the left

lower than expected values based on the former study. The fact that the number of growth zones varies with the depth might be related to a later opening of the deeper fracture or fewer events of fracture reactivation. Model calculations identified a change of groundwater types at approximately 200 m depth at the site (Laaksoharju 2004). It is therefore proposed, that the samples precipitated from different formation waters.

The combination of high Mn content, relatively low Sr content and Chondrite normalized La/Yb, respectively La/Y ratios of the samples from Simpevarp (Table 3) indicates the affiliation of the fracture fillings from drill core KSH01A with generation 5a or 5b/6 calcites, as described by Drake and Tullborg 2009a. This generation has been dated to max. age of ~ 160 Ma (Drake et al. 2017; Ivarsson et al. 2020).

REE adsorption on highly reactive surfaces such as colloids (Ozaki et al. 2006; Pourret et al. 2009) and clay

Table 3 Comparison of Mn and Sr content and Chondrite normalized La/Yb ratios (McDonough and Sun 1995), respectively La/Y ratios of calcite fracture fillings from Simpevarp and Late Palaeozoic frac-ture fillings (Generation5a and 5b/6) from Laxemar and Simpevarp described by Drake and Tullborg 2009a

Site	Simpevarp			Simpevarp/Laxemar	
Depth	205		212	0–686 m	0–686 m
Sample	A	B		Gen. 5a	Gen. 5b/6
Mn (ppm)	Ø 8298	Ø 5800	Ø 2714	147–1980 ppm at KSH01A around 200 m, decreasing with depth from ca. 3000–12,000 ppm to < 100 ppm	
Sr (ppm)	Ø 141	Ø 12	Ø 130	ca. 50–75 ppm	
La/Yb	Ø 53.1	Ø 18	Ø 70.3	Highly variable REE content, mostly flat Chondrite normalized profile	Highly variable REE content, significant LREE enrichment

minerals (Kretzschmar and Schäfer 2005; Bouby et al. 2008; Norrfors et al. 2016) is widely observed in ground waters. The complexation of REE with organic ligands in particular enables the transport of REE with infiltrating waters and leads to an overall increase in the formation water (Torres and Choppin 1984; Xiong 2011). Natural calcites with a Chondrite normalized REE curve depleted in heavy rare-earth elements (HREE) have been linked to precipitation from organic-rich waters under low-temperature conditions in contrast to flat REE profiles which trace back to complexation by inorganic HCO_3^- (Tullborg et al. 2008). Mathurin et al. 2014 applied speciation modeling to show, that the REEs in meteoric groundwaters are strongly bound to humic substances.

It is therefore proposed, that infiltrating surface waters loaded with organic complexes contributed remarkably to the formation waters of overgrowth 2 and 5a at sample KSH01A_205A/B. (see Appendix, Figure 10 and Table 4).

Laxemar

The area scan of sample KLX04_669 from borehole KLX04 reveals a series of four precipitation events. Along the fracture wall, secondary euhedral quartz of ca. 30–50 μm formed followed by three generations of calcite overgrowth. The oldest calcite (zone 1) contains especially high REE contents and relatively high contents of Pb, Th and U. It is disrupted by growth zones 2 and 3 which indicates the disruption of the fracture. The calcite growth zone 2 contains particularly high median Mn and Fe contents. The zone is crossed by numerous micro-veins (calcite growth zone 3), with local accumulations and lamination perpendicular to the growth direction. Parallel and perpendicular fractures in relation to the precipitation front have been linked to crystallization pressure (Noiriel et al. 2010). In comparison to the generation 2 calcite, the micro-veins are enriched in REE with median Chondrite normalized La/Yb ratios of 43.48. Chondrite normalized REE contents reveal an LREE enrichment within the zones 1 and the vein filling carbonate and a flat profile for zone 2. Based on the overall low REE concentration and flat Chondrite normalized profile (see Appendix, Figure 11, Table 6), it is concluded, that the calcites of zones 2 precipitated from formation water with minor share of typically organic-rich surface waters (Torres and Choppin 1984; Xiong 2011).

Samples from borehole KLX19A consist of two generations of calcite. Within the older growth zone 1, TEs are homogeneously distributed. At 414 m, TE contents are elevated along the wall rock/fracture filling contact (most prominent for Na, Th). Within this sample, interspaces between the calcite crystals of growth zone 1 are filled with secondary calcites that are enriched in U but depleted in REE, Sr and Th (see Appendix, Figure 12, Table 7).

Generation 1 calcites are overgrown by large, euhedral calcite crystals, which indicate prolonged and slow precipitation. The μXRF element mapping shows TE incorporation is irregular throughout the growth zone (Fig. 4B). Two crystal-types with clear REE fractionation were identified at 414 m. Type 1 carbonates are enriched in LREE (median Chondrite normalized La/Yb ratio: 26.33) associated with Pb and Th, whereas HREE associated with Mn and Fe are preferentially incorporated in type 2 carbonates (median Chondrite normalized La/Yb ratio: 0.66). At 428 m (Fig. 4A), cluster analysis of the LA-ICP-MS scanned area show three cluster within growth zone 2 with highly differing Fe, Sr, REE, Pb, Th and U contents (Fig. 4D).

The fracture filling generations are divided by a ca. 1-mm-thin greenish contact zone (GCZ) with strongly trace elements enriched rims (Fig. 4C). Low Ca contents indicate other mineral phases than calcite. Maximal difference between LREE and HREE is reached within the rims of the GCZ with median Chondrite normalized La/Yb ratios of 5.5 at 414 m and up to 300 at 428 m.

Deposition of clay minerals and adsorbed TEs seems to be a likely scenario to explain the extremely high TE contents. LREE and TEs such as Th and U predominantly bind on organic ligands and clay minerals. However, in present day fracture waters from bore hole KLX19A, DOC concentrations of 1.5–2.2 mg/l were measured in the corresponding depth. Analogue to present day concentrations, organic ligands have been presumably low in this depth in the past (Laaksoharju et al. 2008b, 2009). The fractionation in association with organic ligands in the formation water seems therefore less probable.

A more likely scenario is the former presence of biofilms. At the Laxemar and Simpevarp sites, paleo-biofilms of estimated Late Pleistocene age were described by Heim et al. 2012. They too linked the accumulations of LREE and TEs (Mg, Al and Fe) to the complexation with organic matter, but also associated them with the transport of Fe-rich colloids (Heim et al. 2012 and references therein). Authigenic clay-minerals, as they are accumulated along the rims of the GCZ, have been proposed to be part of fossilized microbial mats (Sallstedt et al. 2019).

Furthermore, cogenetic calcite and pyrite have been found related to microbial activity (Tullborg et al. 1999; Drake et al. 2015; Drake et al. 2018b). Pyrite precipitation consumes free Fe^{2+} cations in formation waters and could be an explanation for low Fe contents in proximity of the Fe enriched rim of the GCZ at sample KLX19A_428. Cogenetic pyrite has been described as characteristic for generation 5/6 calcites as defined by Drake et al. 2009b. This fact supports the assumption, that calcites investigated in this work precipitated under low-temperature conditions at max. 160 Ma ago (Drake et al. 2017, 2018; Ivarsson et al. 2020).

Thus, the results show that

Fig. 4 **A** Reflected-light microscopy image of sample KLX_19A_428 consisting of granitoid base rock and calcite fracture filling material with the centric greenish contact zone. The µXRF scanned area is outlined in black. **B** µXRF manganese element mapping of the area marked in A). The growth generations one and two are marked with black numbers. The LA-ICP-MS scanned area is outlined in black. **C** LA-ICP-MS manganese element mapping of the area marked in B). Transects cutting the greenish contact zone are marked as white lines within the image (A′–A″, B′–B″). The spatially resolved profiles of Mn, Fe, Sr, La, Yb, Pb, Th, U and Ca are shown below. Trace elements contents are taken from LA-ICP-MS measurements. Calcium contents are calculated from $c\left(Ca^{calcite}\right) = 400,400\ ppm - c\left(TE^{calcite}\right)$ **D** Cluster analysis of the LA-ICP-MS scanned area. Clusters are color coded. Mean trace elements contents of the cluster are displayed normalized to the upper continental crust. Cluster 1 and 2 are mainly found in calcite of the older overgrowth one, as marked in B), cluster 3, 5 and 6 are mainly found in the younger calcite of overgrowth two. Cluster 4 and 7 are part of the greenish contact zone
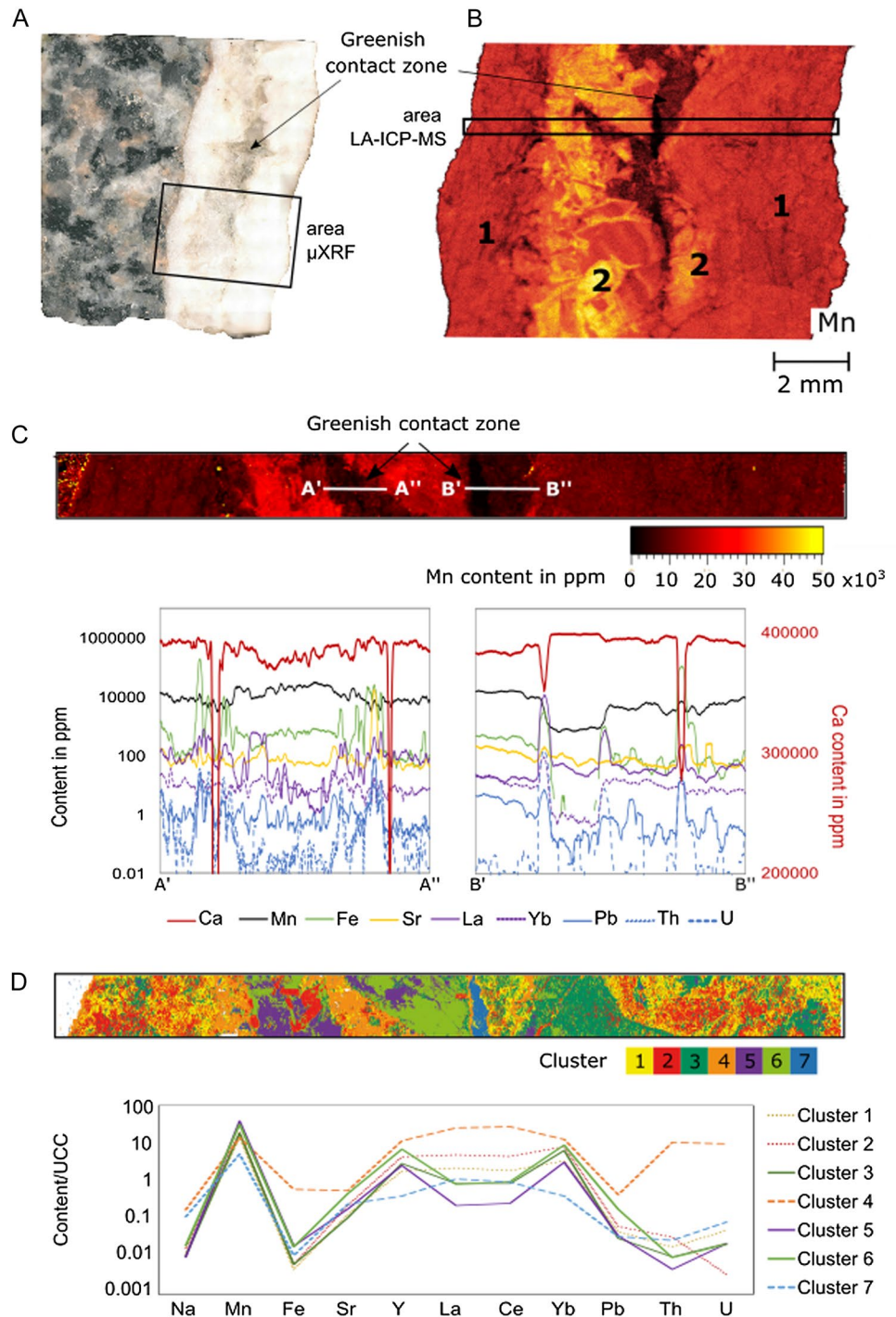
- REE fractionation is highly variable. Chondrite normalized La/Yb ratios reach outliers of < 1 and > 100. However, preferential LREE incorporation is predominating.
- The calcites investigated from Simpevarp (205–212 m depth) presumably belong to generation 5/6 fracture fillings as defined by Drake et al. (2009b).
- The GCZ is a feature of fracture fillings below 400 m at the Simpevarp and Laxemar sites. The zone stands out by extremely high TE contents. The origin of those might result from a combination of coprecipitating minerals in association with biofilms, and the sorption of TEs on inorganic ligands.
- Th contents often lie below the detection limit. In areas where both elements are sufficiently enriched, Th and U follow the same distribution patterns. As a result, uranium which is commonly above detection (mean

of ~ 0.01–0.21 ppm in calcite, ~ 10–24 ppm in GCZ) can be used as a reference for the Th retention capacity in calcites. The similar behavior indicates that Th and U are both present in tetravalent state and therefore coprecipitated in near equilibrium Th/U ratios.

- Throughout this study, REE could be detected in high abundances with values up to 112,233 ppm Y, 283,154 ppm La, 862,177 ppm Ce and 5068 ppm Yb. The retention of trivalent actinides is estimated to be analogously high under comparable hydrogeochemical conditions.

Forsmark

One central line scan and five perpendicularly arranged line scans were carried out at the sample KFM04A_233. The element maps indicate at least one major change in the hydrochemical properties of the formation water. An early generation of highly TE-loaded calcite is followed by a generation with fluctuating TE content. The spatially resolved results show, that the younger growth zone is divided into at least two subzones. Mn and Yb are of higher abundances in closer proximity of growth zone 1. At the center of this overgrowth, light rare-earth elements (LREE) are enriched. Towards the outer rim of zone 2, LREE decrease whereas other TEs such as Fe, Yb, Pb, Th and U reach higher contents (Appendix, Figure 8). However, this study emphasizes the necessity of detailed element mappings to describe the element incorporation precisely and draw differentiated conclusions. Further studies on sample materials from Forsmark are therefore foreseen.

Face-dependent partitioning

The concentric growth zone 4 of sample KSH01_205_A shows areas of distinct TE enrichment (Fig. 5A). These distinctions can be found exclusively within this sample but not at the equivalent growth zone of the same geochronologic episodes within sample KSH01_205_B. This finding indicates sector related zoning as described by Reeder and Paquette (1989) rather than a change in precipitation environment. Within growth zone 4 at least five sectors are visible (Fig. 5A). The statistical analysis confirms the heterogeneity within the growth zone. A cluster analysis of TE contents in the sample assigned the sectors a and b as well as sector B belong to the same cluster, whereas sector A has a uniform signature as growth zone 5a and sector C the same as growth zone 5b (Fig. 5B).

Sector b contains enrichment of the TEs Mn, Fe and Sr, whereas the other TEs compared in this study (Na, Y, La, Ce, Yb, Pb, Th, U) are relatively enriched in sector a. Analogue to growth zone 4, sector B of growth zone 5 stands out by enrichment of divalent TEs. However, sectors A and C do not follow the same pattern. While HREE and U are enriched in sector A, Na, LREE, Pb and Th are enriched in sector C.

Fig. 5 A Element mappings of the sample KSH01A_205_A based on LA-ICP-MS data. Within the Lanthanum map, the concentric growth zones 1–7 are marked. The areas A, B and C as well as a and b mark sectors within the same distinct growth zone. The differentiation of the sectors is based on the trace elements content. **B** Microscopic image of the sample KSH01A_205_A. **C** Average trace elements content of sector a and sector b and sector A, sector B and sector C of growth zone 4, sample KSH01_205_A. Sector A and B show mostly alike composition with slightly increased U and REE (Y, La, Ce, Yb) contents in sector A. Sector C stands out by strong LREE (La, Ce), Pb and Th enrichment. The discrepancy in trace elements contents between sector a and b is most distinguished for LREE (La, Ce) and U
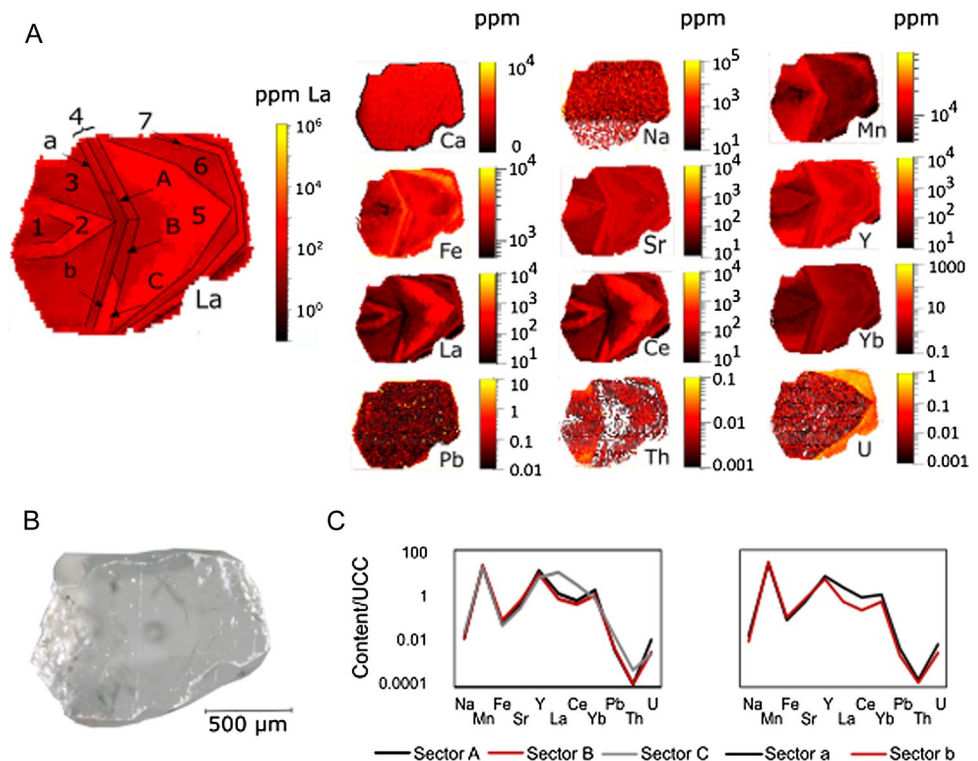
The observations are congruent with the studies of Reeder and Paquette (1989) on synthetic and natural calcite crystals, who found Mn, Fe and Sr to be enriched in the same sector within one growth zone. In addition to these findings, our data suggest, that all other TEs investigated in this study are relatively enriched in the remaining sectors. This observation leads us to the conclusion, that differences in partitioning regarding nonequivalent crystal faces (face dependent partitioning) applies to those elements as well. The structural separation between Mn, Fe, Sr and the trivalent REE (Y, La, Ce and Yb) suggest, that Mn and Fe must be in divalent form. Studies of Elzinga et al. (2002) and Withers et al. (2003) on synthetically grown single-crystal REE-doped calcite show that HREE occur in a six-fold coordination, whereas the incorporation of LREE in the Ca site in calcite requires a sevenfold coordination. The seven-fold coordination, however, leads to disruption of local structures and charge disequilibrium. As one possible mechanism of charge compensation, Elzinga et al. (2002) and Marques Fernandes et al. (2008) refer to co-substitution of Ca^{2+} with monovalent cations, e.g., $Na^+ + REE^{3+}$ as it is most distinct in sector C. From the similar behavior of Pb with LREE and U with HREE it can be reasoned that site-specific partitioning occurs in dependence of the ionic radius.

The face dependent partitioning observed in this study gives strong evidence, that.

- REE (Y, La, Ce, Yb) and divalent cations (Mn, Fe, Sr) do not coprecipitate in the same sector.
- HREE/LREE partitioning might occur. Pb and Th are thereby associated with LREE, U with HREE.

Plausibility assessment of trace element partitioning

Fracture fluids exhibit a unique, depth-dependent compositional fingerprint of the different infiltrating and hydrothermal mixing waters (Gimeno et al. 2008; Drake et al. 2012; Gómez et al. 2014). To allow for the estimation of D_{TE} ratios in natural systems, bulk formation water data are commonly used under the assumption, that the analyzed physicochemical parameters are identically with those of the precipitation solution of the calcites (outermost growth zones of calcites fracture fillings at Laxemar (Drake et al. 2015) have been dated to an age of Late Miocene by Ivarsson et al. (2020). This assumption simplifies not only the temporal fluctuations since the precipitation of the outermost calcite growth zones, but also the spatial disparities between the formation waters in single fractures. However, this approach is still a meaningful addition to laboratory and field derived experiments.

Here, partition coefficients D_{TE} between TE concentration of the formation water and TE content of the outermost overgrowth of single calcite crystals are discussed regarding their plausibility in comparison to laboratory-derived partition coefficients (Curti 1999 and references therein) and previous field studies conducted at the Äspö HRL (Drake et al. 2018 Fig. 6). The latter field studies were carried out on recent precipitated calcites (i.e., 17 years growth period) and recent formation water in bore holes at more than 400 m depth (pH 7.4–7.7, 14 °C) (Drake et al. 2018).

At Simpevarp and Laxemar, two recent groundwater types are dominant in borehole KSH01A (Laaksoharju 2004). The transition between the freshwater type and the underlying brackish groundwater type is located at ca. 200 m. Therefore, data from the formation water of the same borehole section and freshwater type groundwater data taken between 150 and 200 m depth were used to calculate D_{TE} ratios for the samples KSH01A _205_A/B (Table 2, Laaksoharju 2004).

Overall, D_{TE} ratios based on formation water data from < 200 m depth fit best with previously found ratios calculated by Drake et al. (2018) based on 17-year precipitation experiment carried out at the Äspö HRL. Partitioning coefficients of Mn and Fe are comparably higher and lower for Sr when calculated based on formation water data from > 200 m depth. D_{Na} coefficients are in good agreement with field-derived data and at the lower end of laboratory-derived data. REE and U concentrations are only available for formation water > 200 m. The discrepancies of Y uptake between samples from the same site in Simpevarp is striking, as the ratios in 205 m depth match with laboratory-derived ratios while those from 212 m depth correspond with field observations from the area. Partition coefficients for La, Ce and U are in good agreement with laboratory experiments and high in comparison with previous field studies at the Äspö HRL.

For sample KSH01A_212, mean D_{TE} ratios of Mn, Fe and Sr are below or at the low end of the range of laboratory driven values. The low Sr uptake is contrary to previously found ratios at the Äspö area, which even exceed laboratory-derived ratios. Partition coefficients for La and Ce are in good agreement with laboratory experiments and high in comparison with previous field studies. D_{Na} and D_U are in good agreement with field-derived coefficient range.

For sample KFM4A_233 (Forsmark), D_{TE} ratios of Mn, Fe, Sr and U diverge significantly from laboratory and field driven ratios (Fig. 6). Only La and Ce partitioning is in the expected range.

Based on these results, the comparison with partition ratios generated under laboratory conditions should be treated with caution as they are conducted under well-known, abiotic conditions (i.e.; $p = 1 atm, T = 25°C$, defined aqueous speciation, supersaturation conditions, competing cation and others) and therefore represent only a rough approximation of natural systems. Under laboratory conditions, most elements exist in free cationic state, complexation on the other hand is common in the formation waters.

Fig. 6 Partition ratio of the trace elements Na, Mn, Fe, Sr, Y, La, Ce and U between fracture water and outer most growth zone of calcite crystals from bore hole KFM04A (233 m) and KSH01A (205 m and 212 m). For comparison, partition ratios from laboratory experiments carried out at 25 °C and 1 atm (Curti 1999 and references therein) and field-driven experiments carried out at the Äspö HRL (Drake et al. 2018) were added. Missing data are marked in the diagram
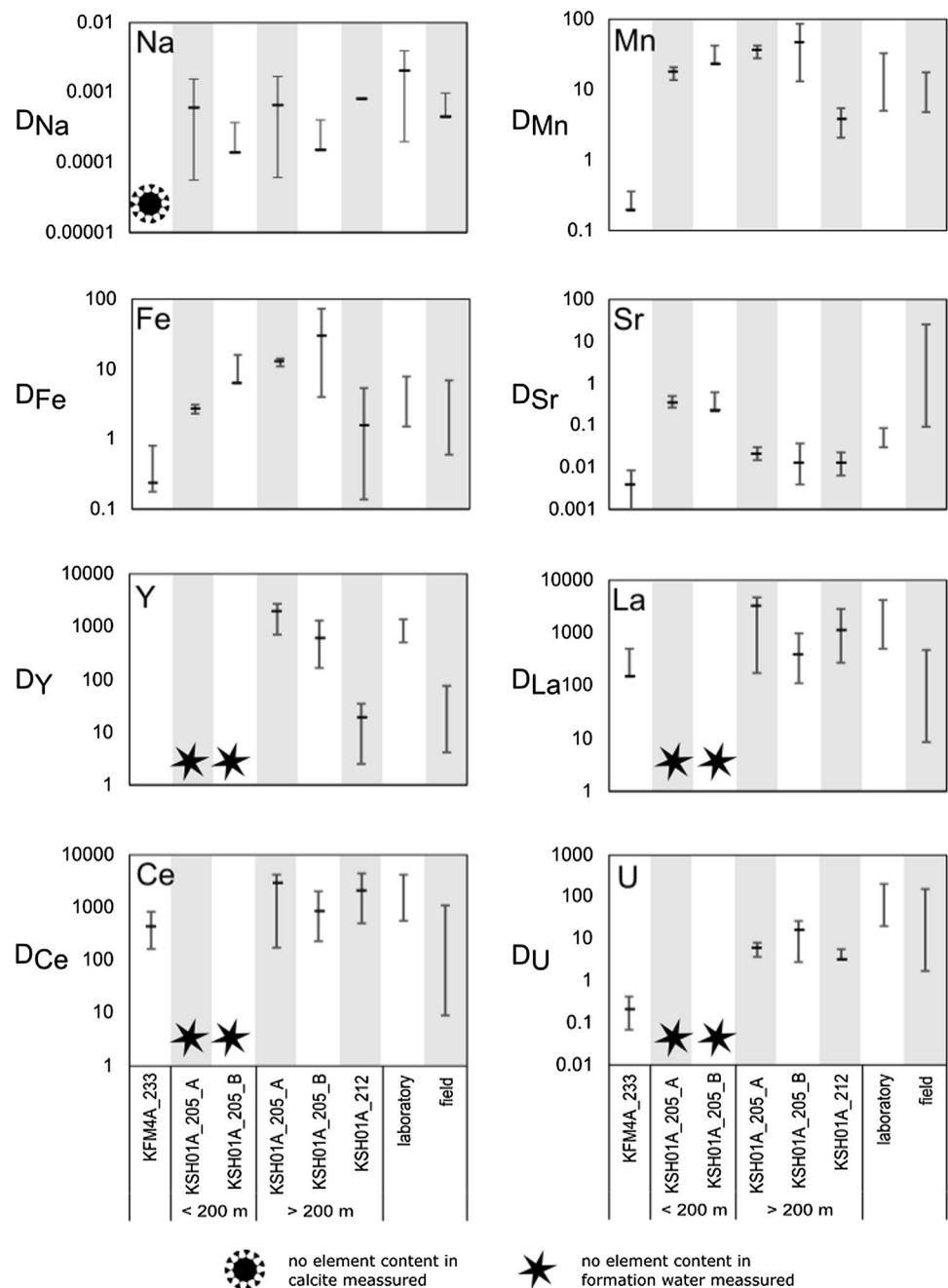
Sr for example is mostly available as Sr^{2+}, Fe mainly as Fe^{2+} and with increasing depth as $FeHS^+$ (Laaksoharju et al. 2009). Mn is available as Mn^{2+}, still a large portion of the element is bound as $MnHS^+$, $MnCO_3$, $MnHCO_3^+$ (Laaksoharju et al. 2009; Kalinowski and Swedish Nuclear Fuel and Waste Management Co., Stockholm 2009). The presence of Mn-reducing microorganisms (Drake et al. 2009; Ivarsson et al. 2020) might lead to local Mn enrichments which could explain the elevated levels in proportion to recent ground waters. With increasing depth (below 250 m), complexation is less relevant due to decreasing HCO_3^- and TOC (total

organic carbon) concentrations in the formation water (Laaksoharju et al. 2009).

As mentioned above, it is unlikely that physiochemical-properties remained comparable since the point of precipitation. However, even with constant trace element concentration, other parameters such as temperature T, pH value and precipitation rate R_P can limit or benefit the TE incorporation. DePaolo (2011) described the influence of these parameters mathematically in Eq. 3. The equation was used in this work, to back-calculate TE/Ca ratios of precipitation solutions and compare them to recentgroundwater data. The example of Sr/Ca and Mn/Ca ratios of the precipitation

solution as a function of log R_P under defined T and pH is given in Fig. 7. The pH values of the recent formation waters range from 7.19 in Forsmark to 7.24 in Simpevarp. We therefore used equilibrium TE/Ca partitioning coefficients of $K_{eq} = 0.035$ for strontium and $K_{eq} = 60$ for manganese and forward kinetic fractionation factor for TE/Ca in the precipitation reaction is $K_f = 0.24$, $R_b = 7 \times 10^{-7}$ mol/m²/sec (values taken from DePaolo (2011) used for experimental data of Lorens (1981) obtained at $T = 25$ °C, pH ≈ 7.4, P = 1 atm).

Under these assumptions, the best fit between recalculated TE/Ca ratios of the precipitation solution and recent ground waters could be found for sample KSH01A_212 and waters from above 200 m under medium to fast precipitation rates (log$Rp \approx$ -5). Even though, Sr/Ca ratios areslightly lower than expected from groundwater data (Fig. 7). For the samples KSH01A_205_A/B and groundwaters above 200 m, Sr/Ca ratios fit with a log$R_P \approx -7$, whereas Mn/Ca ratios would be rather high in comparison to recent groundwaters (power of ten above). However, Mn rich waters are not uncommon at the site (Tullborg et al. 1999). Especially through microbial activity, local Mn enrichments can occur. For groundwater data below 200 m, log$Rp < -8$ is reasonable. The results of KFM04A show, under the given T and pH values, precipitation solution and recent groundwater TE chemistry differ largely.

Overall, these results show, that the partitioning ratios as generated in this and many otherstudies should be handled with caution. The interrelation between D_{TE}, respectively, TE/Ca and R_P given in Fig. 7 shows, that even slight changes

of the precipitation environment can influence significantly the trace element incorporation into the calcite crystal lattice during the secondary phase formation and retention.

Conclusions

The high-resolution maps created in the course of this work allow for the detection of zonation and microstructures within the samples. Local enrichment and variability of elementcontents measured by LA-ICP-MS are in many cases not detectable with μXRF. Thus, it becomes clear, that single point measurements or line scans reveal a limited view of the sample which could lead to misinterpretations. Especially face-dependent partitioning, as it was found at our samples, cannot be covered by point measurements.

From the change of paleo-hydrogeological conditions determined by trace elements, it can be concluded that the retention of rare-earth elements in calcite is high even with fluctuating precipitation conditions. Special attention should be given to the greenish contact zone found in samples from Laxemar at approximately 410–430 m, where clay mineral rims are incorporated into a calcite-dominated aggregate growth. The particularly high trace elements contents in this area are promising in terms of understanding the increased uptake of trace elements.

Taken that lanthanides and trivalent actinides show a similar chemical behavior, and that the observed concentrations and apparent partitioning of the lanthanides in the studied calcites are high, the retention potential of radionuclides in calcite facture fillings in crystalline rock environments for deep geological disposal of radioactive waste should be considered to be promising.

Appendix

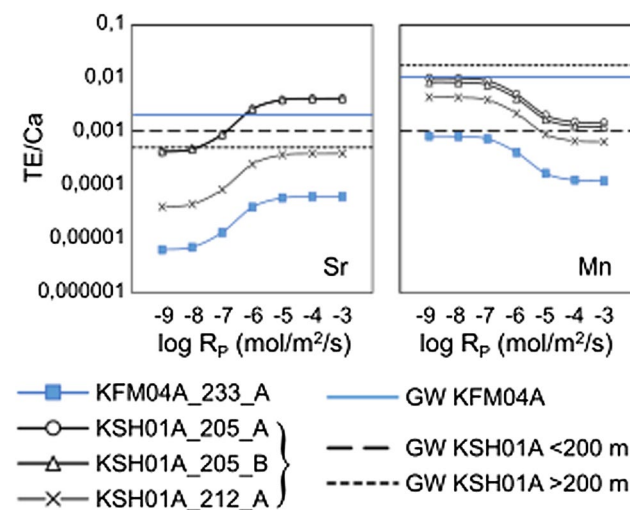## 1. Spatially resolved trace element content in ppm

See Figs. 8 and 9.

Fig. 7 Datapoints mark the recalculated Sr/Ca, respectively Mn/Ca ratios of the precipitation solution in dependency of the precipitation rate R_P as proposed by DePaolo (2011). Calculations are based on the median solid solution Sr/Ca, respectively Mn/Ca ratios of the outermost calcite zones obtained by LA-ICP-MS measurements of samples from bore hole KSH01A (Simpevarp) and KFM04A (Laxemar). pH and T dependent $K_{f,Sr} = 0.24$, $K_{f,Mn} = 5$, $R_b = 7 \times 10$ 7 mol/m²/sec and $K_{eq,Sr} = 0.035$ and $K_{eq,Mn} = 60$ were applied

Fig. 8 Spatially resolved element content of sample KFM04A_233 of the line scans H$_3$ and V based on LA-ICP-MS measurements. For better visualisation moving averages (Period 10) were applied if possible
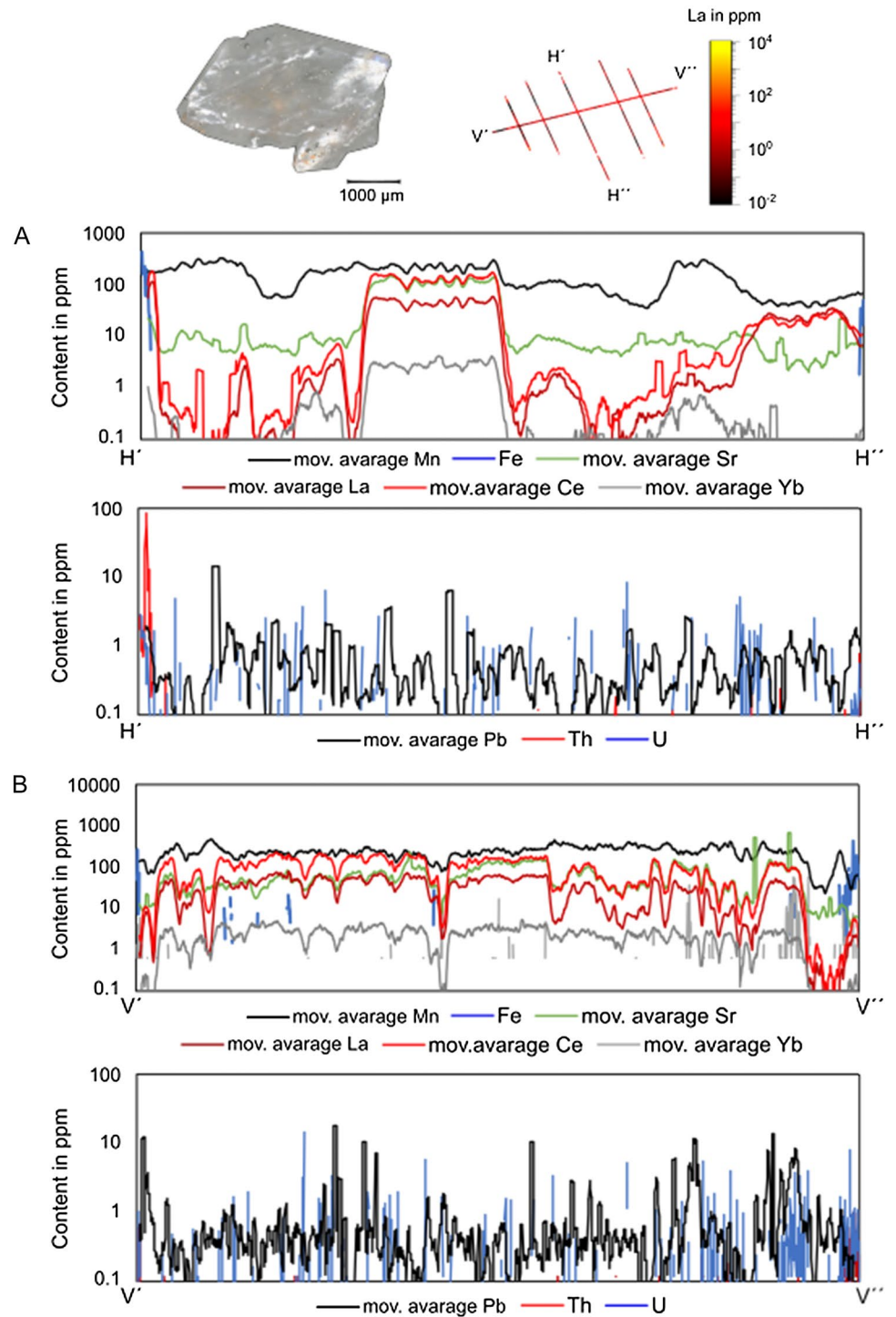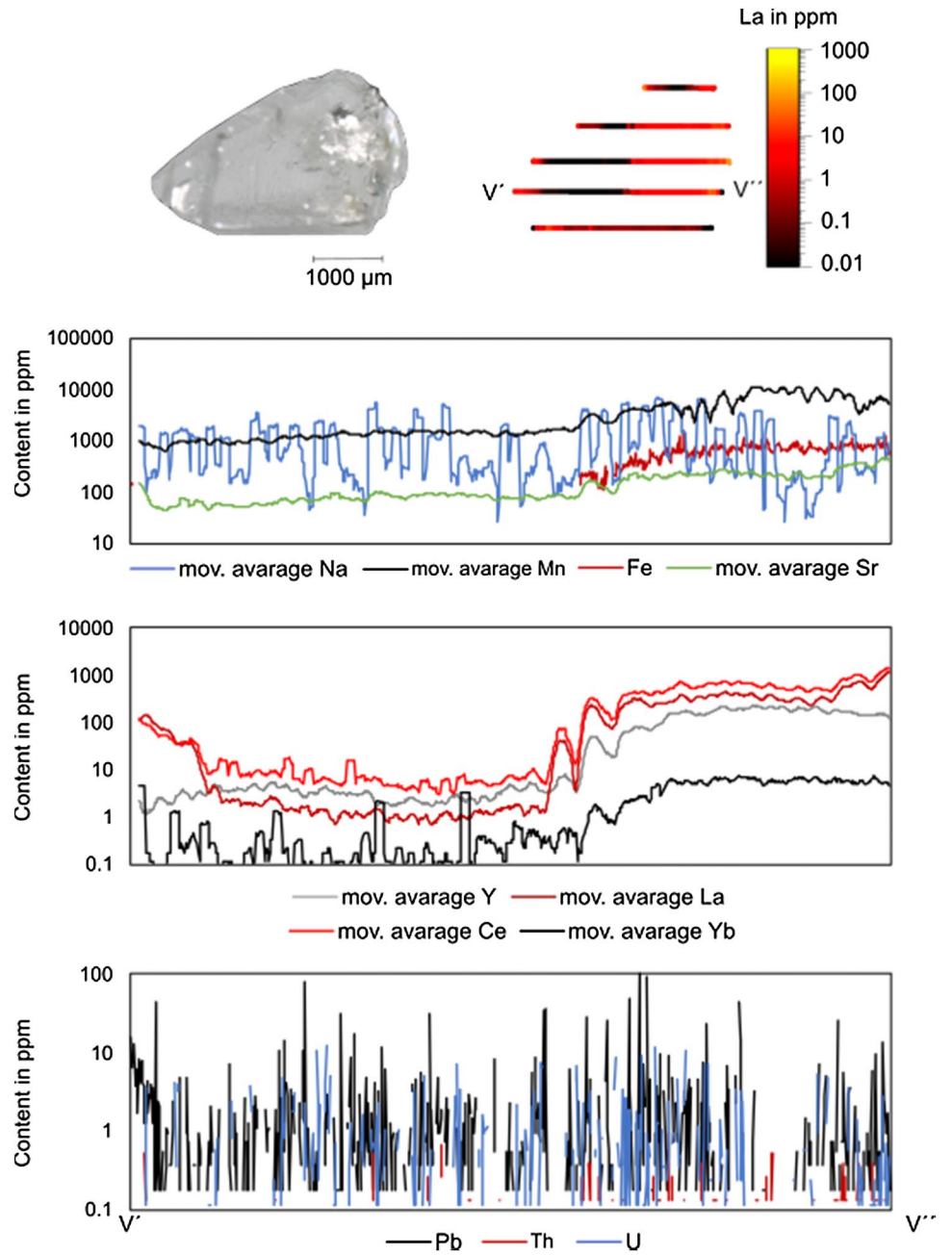
Fig. 9 Spatially resolved element content of sample KSH01A_212 of line scan V based on LA-ICP-MS measurements. For better visualisation moving averages (Period 10) were applied if possible

2. Mean trace-element content based on LA-ICP-MS analysis classified by cluster analysis

See Figs. 10, 11, 12 and 13; Tables 4, 5, 6, 7 and 8.

Fig. 10 Reflected-light microscopy image of sample KSH01_205_A on the left and KSH01A_205_B on the right. Cluster are colour coded on the sample maps next to the image
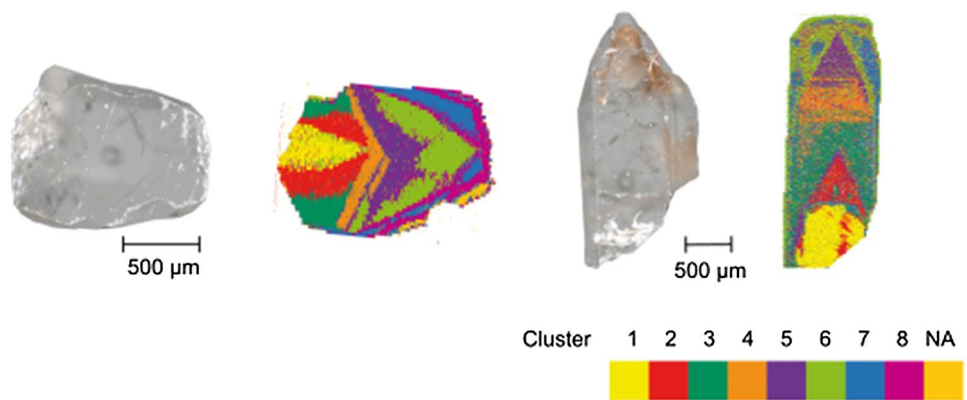
Fig. 11 Reflected-light microscopy image of sample KLX4A_669. Cluster are colour coded on the sample maps next to the image
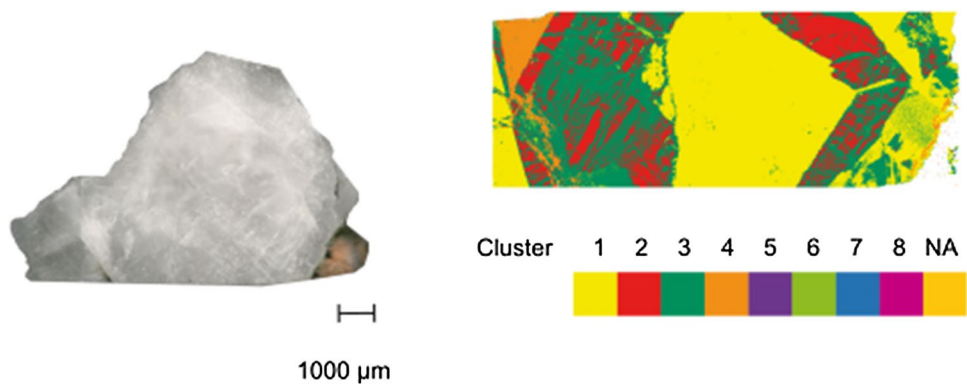

Fig. 12 Reflected-light microscopy image of sample KLX19A_414. Cluster are colour coded on the sample maps next to the image. The cluster WR describes Ca rich wall rock minerals. Consequently, for this sample, calcite cluster 1 starts with a red colour code
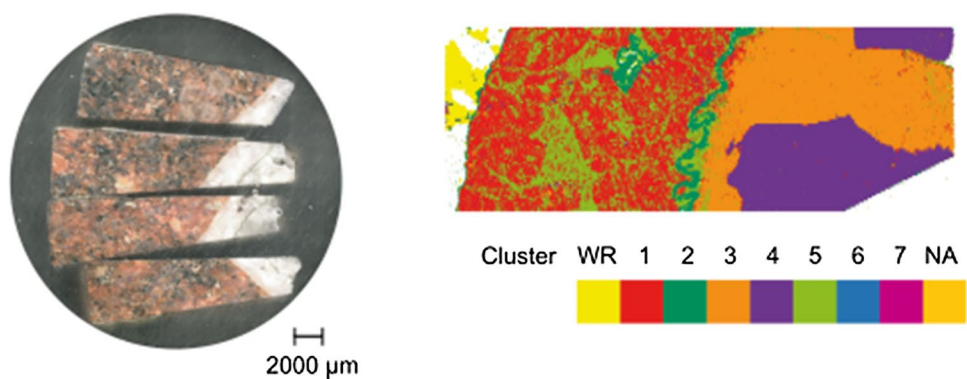

Fig. 13 Reflected-light microscopy image of sample KLX19A_428. Cluster are colour coded on the sample maps next to the image
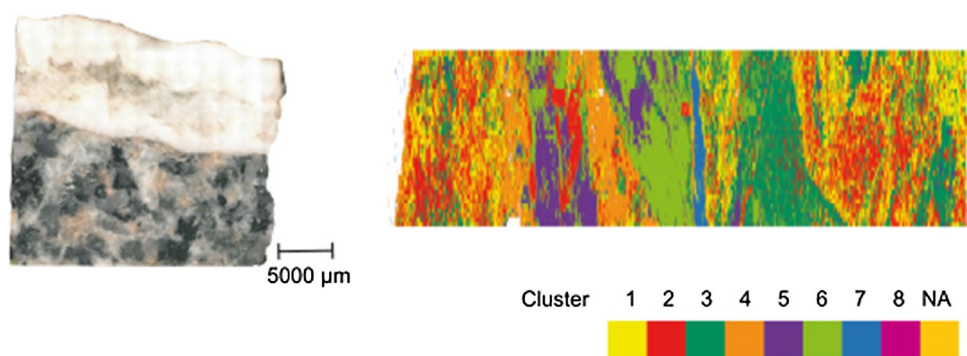
Table 4 Trace element contents of sample KSH01A_205_A based on LA-ICP-MS measurement

	Cluster	N Total	Mean (ppm)	SD	Min. (ppm)	Q1 (ppm)	Median (ppm)	Q3 (ppm)	Max. (ppm)
Na	1	2250	544.6	2186.6	0.4	37.9	53.0	85.1	43,143.2
	2	3304	464.4	2402.1	0.1	22.8	38.8	62.2	71,311.0
	3	1179	880.4	3831.2	0.0	10.1	24.3	144.5	76,984.5
	4	1583	521.8	2195.5	0.2	21.7	38.0	62.0	38,864.8
	5	3189	507.5	2071.0	0.1	26.0	41.3	66.0	39,084.2
	6	4611	571.9	2455.5	0.1	32.8	54.5	81.7	56,013.3
	7	2539	682.1	3322.5	0.0	20.4	46.4	92.3	71,585.6
	8	3397	741.3	3427.0	0.1	28.0	52.6	117.2	107,285.8
Mn	1	2324	7926.5	1795.7	1882.2	6766.4	7907.0	9077.7	15,163.4
	2	3558	12,190.7	2531.1	5113.3	10,701.3	11,998.7	13,354.7	44,023.3
	3	2255	14,435.1	3637.8	5877.1	12,561.7	14,013.0	15,616.7	61,702.4
	4	1992	14,372.0	2609.4	7150.7	12,691.0	14,110.0	15,690.5	37,214.2
	5	3761	9591.5	1789.9	4291.7	8387.3	9331.8	10,544.5	20,171.8
	6	5308	8558.1	1714.4	3524.6	7481.0	8344.8	9328.3	22,485.0
	7	3207	11,274.6	3009.2	4761.7	9264.5	11,042.7	12,961.9	44,325.8
	8	4185	8298.2	1644.6	2703.3	7143.8	8170.5	9278.2	15,859.1
Fe	1	2324	1312.9	406.1	293.4	1064.7	1275.4	1516.1	4937.5
	2	3558	1763.0	544.1	544.6	1455.0	1705.4	1979.8	10,454.1
	3	2255	2061.8	760.6	757.1	1625.6	1983.3	2355.0	21,197.8
	4	1992	3178.4	714.9	1114.8	2742.4	3150.0	3549.6	9817.7
	5	3761	2265.8	498.9	764.7	1929.5	2232.7	2543.4	7054.6
	6	5308	1830.5	408.7	526.6	1551.8	1810.4	2071.1	4854.9
	7	3207	4024.9	2129.6	1253.7	3170.5	3741.3	4526.8	74,181.1
	8	4185	2603.1	658.8	952.6	2185.6	2534.6	2922.5	8935.8
Sr	1	2324	154.2	52.0	21.2	117.2	150.9	184.1	624.3
	2	3558	79.9	18.9	12.6	67.8	78.5	90.1	213.9
	3	2255	72.0	18.5	18.9	59.4	70.7	82.8	150.7
	4	1992	191.4	60.4	48.5	165.2	189.2	214.6	2087.7
	5	3761	174.9	219.6	72.9	146.5	165.3	186.1	12,748.9
	6	5308	121.8	45.6	44.1	100.3	116.8	137.6	2502.2
	7	3207	140.9	46.8	26.4	109.2	133.8	166.7	524.3
	8	4185	141.4	43.4	26.0	113.4	137.5	163.6	967.2
Y	1	2324	93.44	32.39	20.83	75.56	88.03	102.80	508.76
	2	3558	65.72	29.06	13.52	46.33	61.98	79.17	353.60
	3	2255	289.40	121.32	55.59	178.59	288.50	375.51	831.91
	4	1992	124.23	41.51	45.40	95.20	112.79	144.24	341.24
	5	3761	259.79	63.33	89.41	218.63	257.56	295.68	945.36
	6	5308	157.09	40.54	67.67	128.71	151.71	179.75	469.96
	7	3207	188.25	63.30	42.52	143.16	182.33	224.15	581.64
	8	4185	242.69	75.15	41.86	190.64	232.31	284.51	666.86
La	1	2324	106.11	83.86	8.12	35.79	86.49	146.90	745.50
	2	3558	43.78	21.08	4.38	31.96	42.89	51.74	368.71
	3	2255	54.83	22.95	10.68	40.10	53.60	65.53	247.39
	4	1992	37.57	27.69	5.95	18.64	27.01	52.68	351.84
	5	3761	66.45	44.89	15.19	37.67	50.00	80.81	614.03
	6	5308	445.13	150.87	126.20	333.14	446.31	548.06	1160.17
	7	3207	56.82	26.68	5.14	37.05	53.49	72.00	202.08
	8	4185	124.35	70.36	16.65	73.86	110.11	157.29	823.59

Table 4 (continued)

	Cluster	N Total	Mean (ppm)	SD	Min. (ppm)	Q1 (ppm)	Median (ppm)	Q3 (ppm)	Max. (ppm)
Ce	1	2324	70.24	47.62	9.72	29.88	61.38	95.56	509.77
	2	3558	35.65	16.77	3.13	26.62	34.91	42.54	404.00
	3	2255	47.70	18.94	7.16	37.41	46.77	55.39	410.40
	4	1992	29.31	17.30	1.25	17.59	24.24	37.22	220.76
	5	3761	54.56	26.76	10.60	37.84	47.62	63.10	504.90
	6	5308	263.83	97.65	77.59	196.42	258.90	318.70	2680.64
	7	3207	40.13	21.46	2.63	24.51	37.41	52.23	486.04
	8	4185	84.16	43.04	12.56	55.51	75.48	102.37	708.92
Yb	1	2324	0.62	0.31	0.00	0.43	0.58	0.77	2.57
	2	3558	0.53	0.27	0.00	0.34	0.50	0.70	2.63
	3	2255	2.61	1.13	0.60	1.67	2.50	3.34	10.44
	4	1992	0.89	0.42	0.00	0.60	0.83	1.12	6.59
	5	3761	2.28	0.75	0.56	1.78	2.19	2.69	11.17
	6	5308	1.35	0.50	0.12	1.00	1.28	1.63	5.09
	7	3207	1.03	0.48	0.00	0.71	0.96	1.29	5.14
	8	4185	1.59	0.69	0.23	1.08	1.47	1.98	8.00
Pb	1	1676	0.1209	0.5618	0.0000	0.0177	0.0369	0.0799	14.1917
	2	2491	0.1229	1.0366	0.0000	0.0158	0.0326	0.0633	45.9084
	3	1636	0.1962	2.0710	0.0000	0.0163	0.0334	0.0651	63.2961
	4	1382	0.0681	0.2330	0.0000	0.0145	0.0285	0.0506	4.0762
	5	2672	0.1645	2.1400	0.0000	0.0149	0.0306	0.0570	72.5722
	6	3623	0.6349	21.3543	0.0000	0.0149	0.0302	0.0570	1170.6850
	7	2364	0.6834	15.0233	0.0000	0.0161	0.0367	0.0817	533.0561
	8	3119	0.1520	1.2351	0.0000	0.0186	0.0385	0.0841	47.2930
Th	1	401	0.0228	0.0357	0.0071	0.0134	0.0157	0.0234	0.6043
	2	837	0.0242	0.0558	0.0081	0.0138	0.0161	0.0224	1.1525
	3	1180	0.0279	0.0199	0.0066	0.0157	0.0201	0.0346	0.2124
	4	215	0.0192	0.0106	0.0079	0.0137	0.0161	0.0189	0.1003
	5	293	0.0245	0.0252	0.0069	0.0140	0.0164	0.0272	0.3077
	6	1512	0.0203	0.0156	0.0067	0.0135	0.0156	0.0220	0.2259
	7	409	0.0307	0.0524	0.0076	0.0129	0.0159	0.0290	0.7120
	8	839	0.0238	0.0310	0.0065	0.0128	0.0157	0.0253	0.4468
U	1	2324	0.0130	0.0583	0.0002	0.0002	0.0002	0.0048	1.2695
	2	3558	0.0107	0.0452	0.0002	0.0002	0.0002	0.0002	0.8862
	3	2255	0.0153	0.0602	0.0002	0.0002	0.0002	0.0065	1.4816
	4	1992	0.0028	0.0114	0.0002	0.0002	0.0002	0.0002	0.1505
	5	3761	0.0024	0.0074	0.0002	0.0002	0.0002	0.0002	0.1517
	6	5308	0.0127	0.0583	0.0002	0.0002	0.0002	0.0049	2.3589
	7	3207	0.2170	0.1627	0.0002	0.1204	0.1944	0.2786	4.2371
	8	4185	0.1543	0.2327	0.0002	0.0674	0.1166	0.1897	10.0763

Given are mean, standard deviation (SD), minimum (min.), 1st quartile (Q1), median, 3rd quartile (Q3) and maximum (max.)

Table 5 Trace element contents of sample KSH01A_205_B based on LA-ICP-MS measurement

	Cluster	N Total	Mean (ppm)	SD	Min. (ppm)	Q1 (ppm)	Median (ppm)	Q3 (ppm)	Max. (ppm)
Na	1	3228	141.0	929.3	0.0	3.6	9.0	30.2	29,879.3
	2	2239	141.1	841.9	0.0	3.8	8.8	27.8	18,733.2
	3	4553	110.8	723.5	0.0	3.2	7.1	16.8	21,654.9
	4	3776	170.1	1454.1	0.0	4.3	10.4	35.0	66,508.3
	5	2563	179.2	1178.0	0.0	5.1	11.0	28.5	31,391.9
	6	8762	93.2	618.0	0.0	11.4	22.7	47.8	34,207.4
	7	5698	115.2	1603.7	0.0	6.1	12.5	22.8	90,881.6
Mn	1	5052	681.6	483.3	0.1	394.5	544.8	799.7	9363.8
	2	2943	1143.6	575.1	0.0	744.9	1187.9	1555.3	4836.8
	3	6743	5989.1	2273.4	524.9	4694.4	5957.6	7263.3	18,991.3
	4	5799	7984.2	5628.6	223.4	4551.1	6672.3	9700.0	63,456.6
	5	3253	3443.7	2107.9	0.1	2033.6	3264.5	4493.8	19,247.0
	6	9702	5799.5	4296.3	77.9	3642.7	4947.7	6658.9	78,510.1
	7	6854	5321.4	2796.5	62.2	3319.0	5335.2	7090.2	30,392.6
Fe	1	5047	45.8	108.6	0.9	18.5	27.0	43.8	3213.4
	2	3354	367.8	699.3	0.8	87.1	158.7	280.2	12,739.7
	3	6742	888.0	413.8	56.8	620.3	845.5	1090.8	4327.5
	4	5799	1697.5	1165.2	33.2	1031.9	1461.5	2060.3	12,130.8
	5	3294	1093.9	1342.4	56.2	660.8	888.6	1196.4	28,162.8
	6	9702	2305.3	1676.1	83.1	1437.3	1948.5	2642.8	48,978.7
	7	6853	1515.4	840.0	40.4	898.9	1446.0	2058.3	8054.7
Sr	1	5050	4.3	3.1	0.3	2.5	3.4	5.1	63.6
	2	3359	10.4	16.6	1.1	5.8	9.3	13.0	900.7
	3	6742	6.5	3.6	0.4	4.4	5.5	7.3	38.2
	4	5799	17.5	18.9	1.9	10.9	14.9	20.0	1175.1
	5	3294	14.3	10.4	3.5	8.7	11.5	15.9	134.7
	6	9702	12.1	7.1	2.0	7.5	10.5	14.5	160.5
	7	6853	8.3	5.5	0.5	4.8	6.6	10.8	210.8
Y	1	5040	0.71	0.50	0.01	0.39	0.61	0.88	5.92
	2	3355	2.95	4.39	0.07	1.08	1.75	2.60	56.50
	3	6742	3.61	1.99	0.30	2.19	3.23	4.54	18.88
	4	5799	10.15	5.76	0.34	5.91	9.25	13.20	45.57
	5	3294	9.80	9.04	1.30	5.98	8.24	11.27	199.79
	6	9702	15.56	7.14	0.57	10.70	14.24	18.85	76.39
	7	6854	6.06	3.39	0.33	3.29	5.76	8.27	22.06
La	1	4904	0.13	0.19	0.00	0.04	0.07	0.14	4.04
	2	3357	4.42	4.78	0.05	1.66	3.21	5.30	43.79
	3	6741	2.13	1.37	0.06	1.18	1.97	2.72	14.39
	4	5793	2.95	2.01	0.06	1.50	2.47	3.91	15.94
	5	3294	23.71	16.95	2.10	11.35	19.24	33.08	283.65
	6	9702	7.40	8.24	0.58	3.10	4.67	7.81	109.61
	7	6852	2.04	1.63	0.02	1.05	1.68	2.57	16.86
Ce	1	5035	0.46	0.50	0.01	0.20	0.34	0.55	11.60
	2	3359	7.75	7.16	0.27	3.40	5.97	9.22	67.22
	3	6742	4.78	2.75	0.14	2.80	4.60	6.16	27.66
	4	5798	6.87	4.15	0.17	3.93	6.10	8.73	33.12
	5	3294	38.00	25.53	5.81	19.93	32.26	49.61	399.35
	6	9702	13.82	12.50	1.05	6.78	9.93	15.45	163.64
	7	6854	4.31	3.18	0.15	2.21	3.67	5.52	40.95

Table 5 (continued)

	Cluster	N Total	Mean (ppm)	SD	Min. (ppm)	Q1 (ppm)	Median (ppm)	Q3 (ppm)	Max. (ppm)
Yb	1	2991	0.04	0.07	0.01	0.01	0.03	0.04	2.93
	2	3077	0.07	0.10	0.01	0.02	0.04	0.07	1.22
	3	6653	0.09	0.05	0.01	0.05	0.07	0.11	0.48
	4	5358	0.27	0.27	0.02	0.15	0.23	0.35	16.25
	5	3227	0.23	0.19	0.01	0.13	0.19	0.28	3.22
	6	9564	0.28	0.15	0.03	0.18	0.25	0.35	1.95
	7	6733	0.11	0.07	0.01	0.06	0.10	0.15	0.53
Pb	1	3124	0.0204	0.1132	0.0000	0.0029	0.0056	0.0125	2.6266
	2	2179	0.0141	0.1045	0.0000	0.0022	0.0046	0.0092	4.4098
	3	4868	0.0122	0.1083	0.0000	0.0020	0.0040	0.0074	3.9167
	4	4379	0.0890	4.0783	0.0000	0.0033	0.0060	0.0118	267.8140
	5	2395	0.0184	0.1522	0.0011	0.0029	0.0053	0.0104	5.0264
	6	6956	0.0201	0.1395	0.0000	0.0034	0.0061	0.0131	9.2314
	7	5134	0.0123	0.1015	0.0000	0.0020	0.0040	0.0077	3.8232
Th	1	172	0.0050	0.0069	0.0011	0.0018	0.0029	0.0055	0.0701
	2	260	0.0032	0.0032	0.0011	0.0018	0.0021	0.0034	0.0257
	3	1107	0.0026	0.0017	0.0011	0.0017	0.0020	0.0031	0.0224
	4	663	0.0047	0.0060	0.0013	0.0021	0.0033	0.0052	0.1076
	5	633	0.0044	0.0091	0.0012	0.0019	0.0023	0.0041	0.1352
	6	1939	0.0063	0.0119	0.0010	0.0021	0.0036	0.0060	0.3338
	7	984	0.0038	0.0136	0.0008	0.0018	0.0021	0.0036	0.3851
U	1	640	0.0095	0.0223	0.0004	0.0011	0.0030	0.0099	0.4338
	2	442	0.0194	0.0213	0.0005	0.0031	0.0115	0.0291	0.1078
	3	23	0.1120	0.0879	0.0333	0.0521	0.0905	0.1438	0.4009
	4	247	0.0967	0.1167	0.0096	0.0535	0.0816	0.1190	1.7233
	5	92	0.1007	0.1496	0.0035	0.0227	0.0521	0.0950	0.9158
	6	9702	0.0274	0.0256	0.0003	0.0069	0.0223	0.0396	0.3889
	7	6854	0.0143	0.0174	0.0003	0.0010	0.0053	0.0243	0.1156

Given are mean, standard deviation (SD), minimum (min.), 1st quartile (Q1), median, 3rd quartile (Q3) and maximum (max.)

Table 6 Trace element contents of sample KLX4A_699 based on LA-ICP-MS measurement

	Cluster	N Total	Mean (ppm)	SD	Min. (ppm)	Q1 (ppm)	Median (ppm)	Q3 (ppm)	Max. (ppm)
Na	1	179,374	1558.7	18,307.5	0.0	28.3	72.9	207.4	1,556,408.0
	2	57,724	1126.4	17,372.3	0.0	21.8	53.8	141.3	1,411,154.0
	3	126,150	1408.1	19,437.1	0.0	31.3	80.6	231.4	2,374,618.0
Mn	1	261,863	9941.5	2955.2	23.3	8713.5	9962.1	11,196.6	210,957.6
	2	97,587	16,198.9	5387.7	187.5	12,012.4	16,334.0	20,603.5	50,093.2
	3	179,999	14,103.7	5245.5	239.4	11,103.0	14,017.4	17,358.5	154,409.0
Fe	1	261,863	1619.9	32,899.1	5.4	205.2	250.3	289.6	2,657,032.0
	2	97,587	518.7	4154.1	5.7	308.4	433.9	646.9	733,298.8
	3	179,999	1070.9	26,207.3	2.5	246.7	348.3	460.9	3,657,005.0
Sr	1	261,863	83.0	647.2	4.6	52.1	61.9	73.9	171,011.6
	2	97,587	59.8	287.4	12.6	46.9	53.4	61.4	80,826.7
	3	179,999	76.0	427.3	9.2	50.3	61.1	75.1	83,773.7
Y	1	261,863	387.06	715.88	1.07	178.58	411.21	510.92	99,470.52
	2	97,587	2.49	2.60	0.01	0.96	1.92	3.28	179.83
	3	179,999	10.65	12.48	0.01	4.58	7.63	12.82	1054.96
La	1	261,863	110.20	347.00	0.01	61.14	88.91	124.25	46,948.44
	2	97,587	0.12	0.50	0.01	0.01	0.01	0.20	68.81
	3	179,999	7.93	35.34	0.01	0.64	1.28	3.01	3362.55
Ce	1	261,863	248.32	796.27	0.73	153.56	220.57	284.23	113,734.10
	2	97,587	0.50	1.60	0.01	0.01	0.26	0.59	153.48
	3	179,999	12.19	50.80	0.01	1.35	2.55	6.14	11,659.80
Yb	1	261,863	16.56	15.45	0.02	9.70	17.14	22.04	1617.16
	2	97,587	0.16	0.58	0.02	0.02	0.02	0.02	77.11
	3	179,999	0.55	3.00	0.02	0.02	0.02	0.77	1159.52
Pb	1	164,859	3.2094	211.2490	0.0294	0.2164	0.3820	0.7653	75,060.7300
	2	47,577	2.1294	59.0699	0.0365	0.1896	0.3151	0.6160	8008.3330
	3	106,501	2.6189	66.5567	0.0646	0.2202	0.4026	0.8327	9234.1390
Th	1	6423	1.2970	21.5727	0.0487	0.1426	0.1863	0.3071	1190.7100
	2	1199	0.2548	0.4103	0.0668	0.1364	0.1772	0.2769	12.2309
	3	3084	0.3172	0.8533	0.0230	0.1431	0.1822	0.2736	27.8616
U	1	261,863	0.1422	2.7903	0.0026	0.0026	0.0026	0.0026	1037.2400
	2	97,587	0.0882	0.7332	0.0026	0.0026	0.0026	0.0026	52.7842
	3	179,999	0.1092	1.0516	0.0026	0.0026	0.0026	0.0026	200.9853

Given are mean, standard deviation (SD), minimum (min.), 1st quartile (Q1), median, 3rd quartile (Q3) and maximum (max.)

Table 7 Trace element contents of sample KLX19A_414 based on LA-ICP-MS measurement

	Cluster	N Total	Mean (ppm)	SD	Min. (ppm)	Q1 (ppm)	Median (ppm)	Q3 (ppm)	Max. (ppm)
Na	1	49,355	341.3	1471.5	0.0	25.8	51.4	124.1	49,582.5
	2	6788	6307.2	45,117.8	0.9	159.2	402.5	1342.4	1,484,690.0
	3	43,360	272.9	1611.1	0.0	18.9	35.6	72.2	116,980.3
	4	30,546	352.8	3998.0	0.0	13.8	28.4	68.3	597,453.1
	5	30,787	298.2	2138.5	0.0	23.7	46.1	100.7	208,988.3
Mn	1	52,433	8879.2	2027.9	191.5	7564.4	8639.5	9882.8	31,302.0
	2	6793	7736.7	7365.4	144.0	4152.5	5942.2	8470.5	122,462.7
	3	46,767	19,463.0	4294.0	3270.3	16,678.6	19,388.1	21,993.7	61,692.8
	4	34,631	10,331.0	3060.2	168.8	8544.7	10,098.8	11,635.4	226,878.0
	5	32,704	7253.0	2524.5	0.7	5848.4	7011.2	8286.8	28,183.7
Fe	1	52,433	283,4	474.7	30.7	154.2	193.2	269.4	18,657.5
	2	6793	220,578.6	428,424.7	611.1	22,655.1	71,421.7	215,467.6	5,254,798.0
	3	46,767	890.5	757.5	95.9	705.7	843.2	983.1	51,364.6
	4	34,631	413.5	844.8	75.7	253.2	327.2	402.8	75,736.3
	5	32,704	421.5	1277.7	1.5	135.3	183.3	291.7	54,111.4
Sr	1	52,433	75.7	37.3	16.5	56.5	69.7	87.1	1702.2
	2	6793	190.0	905.8	19.9	64.2	89.2	139.0	36,749.5
	3	46,767	129.3	301.9	24.6	81.9	109.4	148.6	35,029.3
	4	34,631	147.2	703.8	17.8	94.3	118.1	152.7	59,820.5
	5	32,704	44.8	22.7	0.2	32.9	41.6	52.2	1466.7
Y	1	52,433	100.64	32.71	27.92	80.48	96.03	115.49	1014.07
	2	6793	94.99	100.22	0.02	43.09	66.06	105.47	1922.18
	3	46,767	189.99	109.45	28.85	147.86	186.84	223.54	7770.80
	4	34,631	118.25	91.49	23.75	82.99	105.83	136.11	4393.30
	5	32,704	57.49	19.04	0.02	45.34	57.26	69.06	719.42
La	1	52,433	65.25	33.70	4.24	42.22	58.73	80.90	986.69
	2	6793	139.30	343.77	4.02	36.46	64.84	133.99	14,626.27
	3	46,767	22.85	16.95	1.24	12.09	18.60	28.04	399.42
	4	34,631	511.58	282.69	9.53	425.36	502.69	575.04	11,520.36
	5	32,704	33.55	29.85	0.02	17.99	27.08	40.53	1609.16
Ce	1	52,433	130.63	97.91	12.68	84.72	112.99	151.73	4425.83
	2	6793	358.76	958.51	13.74	90.53	160.15	333.12	36,508.47
	3	46,767	66.02	62.74	7.09	37.44	54.28	77.03	4672.30
	4	34,631	966.25	810.19	69.04	753.71	892.49	1046.27	45,309.46
	5	32,704	75.39	149.57	0.03	42.44	60.04	84.22	14,847.84
Yb	1	52,433	13.20	5.53	2.07	10.16	12.55	15.44	713.64
	2	6793	11.38	12.08	0.03	4.76	8.01	13.24	173.45
	3	46,767	20.40	19.99	2.63	14.50	19.24	24.58	2836.88
	4	34,631	13.76	8.25	0.03	10.00	12.97	16.60	1140.40
	5	32,704	8.23	3.38	0.03	5.92	7.94	10.20	44.29
Pb	1	49,647	1.4669	29.4332	0.0000	0.3357	0.6023	0.9996	3470.3650
	2	6735	11.0752	180.5259	0.0000	0.9064	2.2339	6.2994	14,657.2400
	3	46,035	1.9944	21.0512	0.0000	0.4635	1.0466	1.9766	2921.2440
	4	33,376	3.3967	113.1067	0.0000	0.3785	0.6663	1.1090	19,262.4000
	5	27,124	1.6299	46.7071	0.0000	0.1612	0.3246	0.5976	6707.7360
Th	1	30,040	0.5272	4.8306	0.0591	0.1401	0.2483	0.4321	652.1945
	2	6644	70.9911	278.0068	0.0366	2.2604	9.1753	41.1631	7153.8940
	3	11,002	0.5505	19.6045	0.0621	0.1234	0.1407	0.2458	2025.9940
	4	6565	3.9655	36.9164	0.0671	0.1308	0.1513	0.2867	1393.6960
	5	14,567	0.4422	4.9485	0.0415	0.1260	0.1748	0.3330	486.4583

Table 7 (continued)

	Cluster	N Total	Mean (ppm)	SD	Min. (ppm)	Q1 (ppm)	Median (ppm)	Q3 (ppm)	Max. (ppm)
U	1	52,433	0.1559	1.3073	0.0034	0.0034	0.0034	0.0910	228.8494
	2	6793	10.4823	24.2576	0.0034	0.5963	2.1258	8.5917	433.2345
	3	46,767	0.1516	0.9016	0.0034	0.0034	0.0034	0.0920	65.0613
	4	34,631	0.2019	1.1074	0.0034	0.0034	0.0034	0.0901	56.4890
	5	32,704	0.2033	1.3179	0.0034	0.0034	0.0034	0.0985	177.2760

Given are mean, standard deviation (SD), minimum (min.), 1st quartile (Q1), median, 3rd quartile (Q3) and maximum (max.)

Table 8 Trace element contents of sample KLX19A_428 based on LA-ICP-MS measurement

	Cluster	N Total	Mean (ppm)	SD	Min. (ppm)	Q1 (ppm)	Median (ppm)	Q3 (ppm)	Max. (ppm)
Na	1	40,712	334.0	1830.4	0.0	70.5	117.6	213.0	117,444.1
	2	39,543	466.5	2966.1	0.0	72.4	128.5	259.0	399,525.2
	3	36,162	282.7	1733.1	0.0	62.7	100.9	168.1	129,777.3
	4	16,374	4513.7	37,490.4	0.2	139.1	261.3	665.3	1,196,845.0
	5	13,442	276.8	4081.8	0.0	51.3	77.5	114.6	294,990.5
	6	23,717	563.3	8896.8	0.1	59.0	93.0	151.2	1,016,395.0
	7	3622	2965.1	34,102.9	0.2	124.7	207.9	335.0	888,626.4
Mn	1	42,932	7508.1	2822.3	648.4	5543.2	7552.2	9309.4	27,515.3
	2	42,996	10,113.5	3060.3	1756.4	8201.9	9821.3	11,674.4	42,310.8
	3	38,944	9781.1	3036.8	1942.6	7778.9	9525.4	11,400.7	37,162.5
	4	16,662	7465.2	6344.9	319.9	4064.6	6443.9	9526.2	304,030.3
	5	14,934	20,467.0	5946.4	2496.0	16,939.9	20,892.0	24,137.2	72,418.6
	6	26,546	16,819.3	4895.7	2573.6	13,719.8	16,317.7	19,310.4	117,181.3
	7	3705	2715.9	3413.5	0.4	821.1	1129.1	2536.7	26,857.4
Fe	1	42,932	140.9	285.1	0.0	69.3	98.0	139.8	15,423.0
	2	42,996	192.4	290.0	0.0	105.2	145.3	207.6	25,411.7
	3	38,944	190.1	315.9	0.0	98.6	151.0	221.5	29,853.4
	4	16,662	18,620.4	77,476.6	9.5	695.3	2405.2	9669.0	2,417,278.0
	5	14,934	584.7	2107.1	13.5	378.9	560.3	703.1	252,379.3
	6	26,546	558.0	1197.4	31.0	343.1	446.4	554.7	102,633.5
	7	3705	330.4	2668.2	0.0	7.5	25.7	81.8	90,355.7
Sr	1	42,932	41.5	18.7	4.8	30.7	38.4	47.9	567.7
	2	42,996	71.7	52.2	11.2	48.7	61.0	79.6	3133.8
	3	38,944	33.8	14.6	3.6	23.2	31.6	42.0	193.3
	4	16,662	175.9	583.6	15.5	53.6	73.7	120.4	20,186.4
	5	14,934	57.3	54.2	6.9	44.7	54.4	66.3	4760.1
	6	26,546	147.0	419.2	22.1	87.2	120.6	169.4	40,252.5
	7	3705	77.4	286.3	0.0	38.8	55.7	75.8	9259.0
Y	1	42,932	37.74	15.89	2.44	26.73	35.41	46.21	170.60
	2	42,996	90.80	216.99	13.33	54.23	71.08	95.33	22,083.24
	3	38,944	60.14	30.06	4.35	39.61	55.95	75.08	962.17
	4	16,662	240.45	1834.94	6.50	55.07	80.23	132.13	112,233.10
	5	14,934	53.30	25.47	0.96	34.73	50.90	69.03	244.11
	6	26,546	144.33	288.80	13.22	96.27	125.18	169.24	21,643.54
	7	3705	8.23	10.07	0.00	2.41	4.75	9.05	115.33
La	1	42,932	71.62	43.74	4.24	42.20	63.67	90.92	2177.05
	2	42,996	159.52	437.41	12.85	71.71	102.60	149.67	21,485.14

Table 8 (continued)

	Cluster	N Total	Mean (ppm)	SD	Min. (ppm)	Q1 (ppm)	Median (ppm)	Q3 (ppm)	Max. (ppm)
	3	38,944	27.60	14.17	1.22	17.38	25.15	35.18	252.44
	4	16,662	823.58	5121.17	9.90	109.65	205.53	446.66	283,154.80
	5	14,934	7.26	4.72	0.02	3.80	6.52	9.72	55.75
	6	26,546	26.49	18.05	2.95	16.43	22.17	30.23	512.12
	7	3705	36.49	55.05	0.02	12.46	25.59	42.06	2265.17
Ce	1	42,932	123.77	79.93	7.49	76.73	110.30	154.09	7314.40
	2	42,996	294.89	1081.84	23.00	129.72	180.11	262.80	96,359.86
	3	38,944	56.45	26.93	3.94	37.42	52.16	70.82	478.12
	4	16,662	1812.04	14,126.97	24.80	207.25	384.21	848.42	862,177.70
	5	14,934	16.92	9.52	0.02	9.62	15.80	22.68	227.20
	6	26,546	63.39	34.80	11.10	41.79	56.59	75.73	984.77
	7	3705	61.18	69.11	0.02	20.90	44.68	72.52	939.34
Yb	1	42,932	5.11	2.76	0.03	3.12	4.68	6.61	34.17
	2	42,996	12.23	26.97	0.75	7.54	10.27	13.95	2848.13
	3	38,944	9.68	9.98	0.61	6.27	8.81	12.06	1618.43
	4	16,662	18.98	93.58	0.03	5.10	8.68	14.13	5067.90
	5	14,934	4.71	2.83	0.03	2.64	4.25	6.31	30.44
	6	26,546	13.46	20.59	0.03	8.57	11.85	16.16	2243.89
	7	3705	0.60	0.89	0.03	0.03	0.03	0.96	11.13
Pb	1	31,813	1.0587	27.0439	0.0705	0.2415	0.4266	0.7112	3547.2460
	2	37,487	1.2172	9.6752	0.0983	0.3971	0.7012	1.1743	939.1515
	3	26,510	0.7564	3.4037	0.0645	0.2436	0.4224	0.7219	212.0463
	4	15,686	7.8645	66.7598	0.1132	0.7134	1.5044	3.7996	7580.7270
	5	11,660	0.7723	7.6163	0.0939	0.2581	0.4864	0.8063	806.8278
	6	25,691	3.1291	51.2807	0.1093	1.0681	2.0290	3.3756	7650.1890
	7	1692	1.2533	7.0501	0.0892	0.2378	0.3575	0.6717	146.2635
Th	1	17,945	0.4392	1.1754	0.0587	0.1920	0.2524	0.4370	70.2832
	2	22,743	0.6362	1.9338	0.0947	0.2352	0.3619	0.6289	106.6625
	3	10,403	0.3782	1.3379	0.0626	0.1936	0.2435	0.3865	74.4016
	4	14,961	121.1233	1695.0840	0.1073	1.3290	4.6241	15.3572	85,290.4800
	5	1989	0.3545	1.5402	0.0283	0.1918	0.2241	0.2733	63.9064
	6	5950	0.4303	1.1068	0.0985	0.2097	0.2492	0.4017	47.9916
	7	516	1.9994	5.5256	0.0881	0.2374	0.3649	1.1651	54.3225
U	1	42,932	0.1230	1.6656	0.0000	0.0000	0.0000	0.0000	214.3815
	2	42,996	0.0084	0.1224	0.0000	0.0000	0.0000	0.0000	13.3082
	3	38,944	0.0559	0.6415	0.0000	0.0000	0.0000	0.0000	34.8827
	4	16,662	24.1402	220.4716	0.0000	0.6672	2.4482	8.1514	11,006.2100
	5	14,934	0.0546	0.9132	0.0000	0.0000	0.0000	0.0000	87.3487
	6	26,546	0.0520	0.4885	0.0000	0.0000	0.0000	0.0000	21.5119
	7	3705	0.2044	1.0103	0.0000	0.0000	0.0000	0.0000	27.3483

Given are mean, standard deviation (SD), minimum (min.), 1st quartile (Q1), median, 3rd quartile (Q3) and maximum (max.)

3. Example: limit of detection

See Table 9.

Table 9 Limit of detection of the LA-ICP-MS scans of sample KLX19A_428

	Min. (ppm)	Max. (ppm)
^{23}Na	6.5	19
^{55}Mn	0.48	1.1
^{56}Fe	3.3	8.9
^{88}Sr	0.011	0.058
^{89}Y	0.022	0.14
^{139}La	0.014	0.034
^{140}Ce	0.011	0.027
^{172}Yb	0.036	0.09
^{208}Pb	0.01	0.083
^{232}Th	0.0091	0.023
^{238}U	0.0068	0.017

Data availability All relevant data are included. Please contact the authors for further access to data and images.

Code availability Not applicable.

Declarations

Conflict of interest The authors declare that they have no competing interests.

References

Andersson J, Skagius K, Winberg A, Lindborg T, Ström A (2013) Site-descriptive modelling for a final repository for spent nuclear fuel in Sweden. Environ Earth Sci 69(3):1045–1060. https://doi.org/10.1007/s12665-013-2226-1

Bouby M, Geckeis H, Geyer FW (2008) Application of asymmetric flow field-flow fractionation (AsFlFFF) coupled to inductively coupled plasma mass spectrometry (ICPMS) to the quantitative characterization of natural colloids and synthetic nanoparticles. Anal Bioanal Chem 392(7):1447–1457. https://doi.org/10.1007/s00216-008-2422-0

Bruno J, Sandino A (1987): Radionuclide co-precipitation. Edited by Swedish nuclear fuel and waste management Co., Stockholm. Sweden. https://www.skb.com/publication/3266/TR87-23webb.pdf. SKB Report TR-87-23; IAEA Reference Number 19071400

OECD/NEA (2007) Chemical Thermodynamics of Solid Solutions of Interest in Radioactive Waste Management, Vol 10, Chemical Thermodynamics, OECD Publishing, Paris. https://doi.org/10.1787/9789264033191-en

Brydsten L, Strömgren M (2010) A coupled regolith-lake development model applied to the Forsmark site. Edited by Swedish nuclear fuel and waste management Co., Stockholm. Sweden. https://www.skb.com/publication/1938957/TR-09-21.pdf

Chou L, Garrels RM, Wollast R (1989) Comparative study of the kinetics and mechanisms of dissolution of carbonate minerals. Chem Geol 78(3):269–282. https://doi.org/10.1016/0009-2541(89)90063-6

Curti E (1999) Coprecipitation of radionuclides with calcite: estimation of partition coefficients based on a review of laboratory investigations and geochemical data. Appl Geochem 14(4):433–445. https://doi.org/10.1016/S0883-2927(98)00065-1

Day CC, Henderson GM (2013) Controls on trace-element partitioning in cave-analogue calcite. Geochim et Cosmochim Acta 120:612–627. https://doi.org/10.1016/j.gca.2013.05.044

DePaolo DJ (2011) Surface kinetic model for isotopic and trace element fractionation during precipitation of calcite from aqueous solutions. Geochim et Cosmochim Acta 75(4):1039–1056. https://doi.org/10.1016/j.gca.2010.11.020

Dobashi R, Shikazono N (2008) Geochemical study of rare earth elements in carbonate minerals in sedimentary rocks around Tono uranium deposit, central Japan. An example of natural analogue study of geological disposal of high-level nuclear waste. Chikyu Kagaku 42(3):79–98; IAEA Reference Number 40008942. https://inis.iaea.org/search/search.aspx?orig_q=RN:40008942.

Drake H, Tullborg E-L (2009a) Paleohydrogeological events recorded by stable isotopes, fluid inclusions and trace elements in fracture minerals in crystalline rock, Simpevarp area, SE Sweden. Appl Geochem 24(4):715–732. https://doi.org/10.1016/j.apgeochem.2008.12.026

Drake H, Tullborg E-L, Page L (2009b) Distinguished multiple events of fracture mineralisation related to far-field orogenic effects in Paleoproterozoic crystalline rocks, Simpevarp area, SE Sweden. Lithos 110(1):37–49. https://doi.org/10.1016/j.lithos.2008.12.003

Drake H, Tullborg E-L, Hogmalm KJ, Åström ME (2012) Trace metal distribution and isotope variations in low-temperature calcite and groundwater in granitoid fractures down to 1 km depth. Geochim

et Cosmochim Acta 84:217–238. https://doi.org/10.1016/j.gca.2012.01.039

Drake H, Åström ME, Heim C, Broman C, Åström J, Whitehouse M et al (2015) Extreme ^{13}C depletion of carbonates formed during oxidation of biogenic methane in fractured granite. Nat Commun. https://doi.org/10.1038/ncomms8020

Drake H, Heim C, Roberts NMW, Zack T, Tillberg M, Broman C et al (2017) Isotopic evidence for microbial production and consumption of methane in the upper continental crust throughout the phanerozoic eon. Earth Planet Sci Lett 470:108–118. https://doi.org/10.1016/j.epsl.2017.04.034

Drake H, Mathurin FA, Zack T, Schäfer T, Roberts NMW, Whitehouse M et al (2018) Incorporation of metals into calcite in a deep anoxic granite aquifer. Environ Sci Technol 52(2):493–502. https://doi.org/10.1021/acs.est.7b05258

Drake H, Sandström B, Tullborg E-L (2006) Mineralogy and geochemistry of rocks and fracture fillings from Forsmark and Oskarshamn: compilation of data for SR-Can. Edited by Swedish nuclear fuel and waste management Co., Stockholm, Sweden. SKB Report R-06-109; IAEA Reference Number38041832. https://www.skb.com/publication/1233994/R-06-109.pdf

Eisenbud M, Krauskopf K, Franca EP, Lei W, Ballad R, Linsalata P, Fujimori K (1984) Natural analogues for the transuranic actinide elements: an investigation in Minas Gerais, Brazil. Environ Geol Water Sci 6(1):1–9. https://doi.org/10.1007/BF02525564

Elzinga E, Reeder RJ, Withers SH, Peale R, Mason RA, Beck KM, Hess W (2002) EXAFS study of rare-earth element coordination in calcite. Geochim et Cosmochim Acta 66:2875–2885. https://doi.org/10.1016/S0016-7037(02)00888-8

Fernandes Marques M, Schmidt M, Stumpf T, Walther C, Bosbach D, Klenze R, Fanghänel T (2008) Site-selective time-resolved laser fluorescence spectroscopy of Eu3+ in calcite. J Colloid Interface Sci 321(2):323–331. https://doi.org/10.1016/j.jcis.2008.01.017

Füger A, Konrad F, Leis A, Dietzel M, Mavromatis V (2019) Effect of growth rate and pH on lithium incorporation in calcite. Geochim et Cosmochim Acta 248:14–24. https://doi.org/10.1016/j.gca.2018.12.040

Gimeno MJ, Auque LF, Gomez JB, Acero P (2008) Water-rock interaction modelling and uncertainties of mixing modelling SDM-Site Forsmark. Edited by Swedish nuclear fuel and waste management Co., Stockholm. Sweden. 1402–3091. SKB Report R-08-86; IAEA Reference Number 39121604. https://www.skb.com/publication/1730598/R-08-86.pdf

Gómez JB, Gimeno MJ, Auqué LF, Acero P (2014) Characterisation and modelling of mixing processes in groundwaters of a potential geological repository for nuclear wastes in crystalline rocks of Sweden. Sci Total Environ 468–469:791–803. https://doi.org/10.1016/j.scitotenv.2013.09.007

Guenthner WR, Reiners PW, Drake H, Tillberg M (2017) Zircon, titanite, and apatite (U-Th)/He ages and age-eU correlations from the Fennoscandian Shield, southern Sweden. Tectonics 36(7):1254–1274. https://doi.org/10.1002/2017TC004525

Hedin A (2006) Long-term safety for KBS-3 repositories at Forsmark and Laxemar—a first evaluation. Main report of the SR-Can project. Edited by Swedish Nuclear Fuel and Waste Management Co., Stockholm. Sweden. https://www.skb.com/publication/1192585/TR-06-09.pdf

Heim C, Lausmaa J, Sjövall P, Toporski J, Dieing T, Simon KEA et al (2012) Ancient microbial activity recorded in fracture fillings from granitic rocks (Äspö Hard Rock Laboratory, Sweden). Geobiology 10(4):280–297. https://doi.org/10.1111/j.1472-4669.2012.00328.x

Henderson LM, Kracek FC (1927) The fractional precipitation of barium and radium chromatomes. J Am Chem Soc 49(3):738–749. https://doi.org/10.1021/ja01402a017

Hermansson T, Stephens MB, Corfu F, Andersson J, Page L (2007) Penetrative ductile deformation and amphibolite-facies metamorphism prior to 1851 Ma in the western part of the Svecofennian orogen. Fennosc Shield Precambrian Res 153(1):29–45. https://doi.org/10.1016/j.precamres.2006.11.009

Högdahl K, Andersson UB, Eklund O (2004) The Transscandinavian igneous belt (TIB) in Sweden: a review of its character and evolution. Special Paper Geol Survey of Finland 37:1–125

Ivarsson M, Drake H, Neubeck A, Sallstedt T, Bengtson S, Roberts NMW, Rasmussen B (2020) The fossil record of igneous rock. Earth-Sci Rev 210:103342. https://doi.org/10.1016/j.earscirev.2020.103342

Johannesson KH, Stetzenbach KJ, Hodge VF (1995) Speciation of the rare earth element Neodymium in groundwaters of the Nevada test site and Yucca Mountain and implications for actinide solubility. Appl Geochem 10(5):565–572. https://doi.org/10.1016/0883-2927(95)00028-3

Joyce M (ed) (2017) Nuclear engineering. A conceptual introduction to nuclear power. 1st ed.: Butterworth-Heinemann. https://www.elsevier.com/books/nuclear-engineering/joyce/978-0-08-100962-8

Kalinowski BE, Swedish Nuclear Fuel and Waste Management Co., Stockholm (eds) (2009) Background complementary hydrogeochemical studies. Site descriptive modelling SDM-Site Laxemar. With assistance of David A. Amphos, Lara D. Amphos, Mel Gascoyne, Ioana Gurban, Jorge Molinero, Ann-Chatrin Nilsson et al. Sweden. https://www.skb.se/publikation/1984968/R-08-111.pdf

Krauskopf KB (1986) Thorium and rare-earth metals as analogs for actinide elements. Chem Geol 55(3):323–335. https://doi.org/10.1016/0009-2541(86)90033-1

Kretzschmar R, Schäfer T (2005) Metal retention and transport on colloidal particles in the environment. Elements 1(4):205–210. https://doi.org/10.2113/gselements.1.4.205

Kwon S, Cho WJ, Han PS (2006) Concept development of an underground research tunnel for validating the Korean reference HLW disposal system. Tunn Underground Space Technol 21(2):203–217. https://doi.org/10.1016/j.tust.2005.06.008

Laaksoharju M, Gascoyne M, Gurban I (2008a) Understanding groundwater chemistry using mixing models. Appl Geochem 23(7):1921–1940. https://doi.org/10.1016/j.apgeochem.2008.02.018

Laaksoharju M, Smellie J, Tullborg E-L, Gimeno MJ, Hallbeck L, Molinero J, Waber HN (2008b) Bedrock hydrogeochemistry Forsmark. Site descriptive modelling SDM-Site Forsmark. Edited by Swedish Nuclear Fuel and Waste Management Co., Stockholm. Sweden. https://www.skb.com/publication/1841127/R-08-47.pdf. SKB Report R-08-47, IAEA Reference Number 40042536

Laaksoharju M, Smellie J, Tullborg E-L, Gimeno M, Molinero J, Gurban I, Hallbeck L (2008c) Hydrogeochemical evaluation and modelling performed within the Swedish site investigation programme. Appl Geochem 23(7):1761–1795. https://doi.org/10.1016/j.apgeochem.2008.02.015

Laaksoharju M, Smellie J, Tullborg E-L, Wallin B, Drake H, Gascoyne M et al (2009) Bedrock hydrogeochemistry Laxemar. Site descriptive modelling SDM-Site Laxemar. Edited by Swedish Nuclear Fuel and Waste Management Co., Stockholm. Sweden. SKB Report R-08-93. https://www.skb.com/publication/1941366/R-08-93.pdf

Laaksoharju M, Smellie J, Gimeno M, Auque L, Gomez J, Tullborg E-L, Gurban I (2004) Hydrogeochemical evaluation of the Simpevarp area, model version 1.1. Sweden. SKB Report R-04-05; IAEA Reference Number 35089220. https://www.osti.gov/etdeweb/servlets/purl/20521174

Landström O, Tullborg E-L (1995) Interactions of trace elements with fracture filling minerals from the Äspö Hard Rock Laboratory. Edited by Swedish Nuclear Fuel and Waste Management Co., Stockholm. Sweden (0284–3757). SKB Report TR-95-13; IAEA

Reference Number 27011416. https://www.inis.iaea.org/search/search.aspx?orig_q=RN:27011416

Laverov NP, Yudintsev SV, Kochkin BT, Malkovsky VI (2016) The russian rtrategy of using crystalline rock as a repository for nuclear waste. Elements 12(4):253–256. https://doi.org/10.2113/gselements.12.4.253

Lorens RB (1981) Sr, Cd, Mn and Co distribution coefficients in calcite as a function of calcite precipitation rate. Geochim et Cosmochim Acta 45(4):553–561. https://doi.org/10.1016/0016-7037(81)90188-5

Lundin L, Lode E, Stendahl J, Melkerud P-Ar, Bjoerkvald L, Thorstensson A (2004) Soils and site types in the Forsmark area. Edited by Swedish Nuclear Fuel and Waste Management Co., Stockholm. Sweden (1402–3091). SKB Report R-04-08; IAEAReference Number 35072465.http://inis.iaea.org/search/search.aspx?orig_q=RN:35072465

Maskenskaya OM, Drake H, Mathurin FA, Åström ME (2015) The role of carbonate complexes and crystal habit on rare earth element uptake in low-temperature calcite in fractured crystalline rock. Chem Geol 391:100–110. https://doi.org/10.1016/j.chemgeo.2014.10.030

Mathurin FA, Åström ME, Drake H, Maskenskaya OM, Kalinowski BE (2014) REE and Y in groundwater in the upper 1.2 km of proterozoic granitoids (Eastern Sweden)—assessing the role of composition and origin of groundwaters, geochemistry of fractures, and organic/inorganic aqueous complexation. Geochim et Cosmochim Acta 144:342–378. https://doi.org/10.1016/j.gca.2014.08.004

McDonough WF, Sun S (1995) The composition of the earth. Chem Geol 120(3):223–253. https://doi.org/10.1016/0009-2541(94)00140-4

Milnes AG, Stephens MB, Wahlgren C-H, Wikström L (2008) Geoscience and high-level nuclear waste disposal: the Nordic scene. Int Union Geol Sci 31(1):168–175. https://doi.org/10.18814/epiiugs/2008/v31i1/023

Milodowski AE, Bath A, Norris S (2018) Palaeohydrogeology using geochemical, isotopic and mineralogical analyses: salinity and redox evolution in a deep groundwater system through quaternary glacial cycles. Appl Geochem 97:40–60. https://doi.org/10.1016/j.apgeochem.2018.07.008

Mizuno T, Milodowski AE, Iwatsuki T (2022) Precipitation sequence of fracture-filling calcite in fractured granite and changes in the fractionation process of rare earth elements and yttrium. Chem Geol. https://doi.org/10.1016/j.chemgeo.2022.120880

Noiriel C, Renard F, Doan M-L, Gratier J-P (2010) Intense fracturing and fracture sealing induced by mineral growth in porous rocks. Chem Geol 269(3):197–209. https://doi.org/10.1016/j.chemgeo.2009.09.018

Norrfors KK, Marsac R, Bouby M, Heck S, Wold S, Lützenkirchen J, Schäfer T (2016) Montmorillonite colloids: II. Colloidal size dependency on radionuclide adsorption. Appl Clay Sci 123:292–303. https://doi.org/10.1016/j.clay.2016.01.017

Nyman H, Sohlenius G, Strömgren M, Brydsten L (2008) Depth and stratigraphy of regolith site descriptive modelling SDM-Site Laxemar. Edited by Swedish Nuclear Fuel and Waste Management Co., Stockholm. Sweden (1402–3091). SKB Report R-08-06; IAEA Reference Number 40042512. http://inis.iaea.org/search/search.aspx?orig_q=RN:40042512

Ojovan MI, Lee William EK, Stepan N (2019) An Introduction to Nuclear Waste Immobilisation: Elsevier Science. ISBN 9780081027035. https://www.elsevier.com/books/an-introduction-to-nuclear-waste-immobilisation/ojovan/978-0-08-102702-8

Ozaki T, Suzuki Y, Nankawa T, Yoshida T, Ohnuki T, Kimura T, Francis AJ (2006) Interactions of rare earth elements with bacteria and organic ligands. J Alloys Compd 408–412:1334–1338. https://doi.org/10.1016/j.jallcom.2005.04.142

Pourret O, Gruau G, Dia A, Davranche M, Molénat J (2009) Colloidal control on the distribution of rare earth elements in shallow groundwaters. Aquatic Geochem 16(1):31. https://doi.org/10.1007/s10498-009-9069-0

Quinto F, Blechschmidt I, Garcia Perez C, Horst G, Frank G, Robin et al (2017) Multiactinide analysis with accelerator mass spectrometry for ultratrace determination in small samples: application to an in situ radionuclide tracer test within the colloid formation and migration experiment at the grimsel test site (Switzerland). Anal Chem 89(13):7182–7189. https://doi.org/10.1021/acs.analchem.7b01359

Reeder RJ, Paquette J (1989) Sector zoning in natural and synthetic calcites. Sedimentary Geol 65(3):239–247. https://doi.org/10.1016/0037-0738(89)90026-2

Rouff AA, Elzinga EJ, Reeder RJ, Fisher NS (2005) The influence of pH on the kinetics, reversibility and mechanisms of Pb(II) sorption at the calcite-water interface. Geochim et Cosmochim Acta 69(22):5173–5186. https://doi.org/10.1016/j.gca.2005.04.022

Saintot A, Stephens MB, Viola G, Nordgulen Ø (2011) Brittle tectonic evolution and paleostress field reconstruction in the southwestern part of the Fennoscandian Shield, Forsmark, Sweden. Tectonics. https://doi.org/10.1029/2010TC002781

Sallstedt T, Ivarsson M, Drake H, Skogby H (2019) Instant attraction: clay authigenesis in fossil fungal biofilms. Geosciences. https://doi.org/10.3390/geosciences9090369

Sandström B, Tullborg E-L, Smellie J, MacKenzie AB, Suksi J (2008) Fracture mineralogy of the Forsmark site. SDM-Site Forsmark. Edited by Swedish Nuclear Fuel and Waste Management Co., Stockholm. Sweden (1402–3091). SKB Report R-08-102; IAEA ReferenceNumber 39121601.https://inis.iaea.org/collection/NCLCollectionStore/_Public/39/121/39121601.pdf

SKB (2008) Geological evolution, palaeoclimate and historical development of the Forsmark and Laxemar-Simpevarp areas. Site descriptive modelling SDM-Site. Edited by Björn Söderbäck, Swedish Nuclear Fuel and Waste Management Co., Stockholm. Sweden (1402–3091). SKB Report R-08-19; IAEA Reference Number 40015709. http://inis.iaea.org/search/search.aspx?orig_q=RN:40015709

Smellie JAT, Karlsson F (1999) The use of natural analogues to assess radionuclide transport. Eng Geol 52(3):193–220. https://doi.org/10.1016/S0013-7952(99)00006-X

Smrzka D, Zwicker J, Bach W, Feng D, Himmler T, Chen D, Peckmann J (2019) The behavior of trace elements in seawater, sedimentary pore water, and their incorporation into carbonate minerals: a review. Facies 65(4):41. https://doi.org/10.1007/s10347-019-0581-4

Söderlund U, Isachsen CE, Bylund G, Heaman LM, Jonathan Patchett P, Vervoort JD, Andersson UB (2005) U-Pb baddeleyite ages and Hf, Nd isotope chemistry constraining repeated mafic magmatism in the Fennoscandian Shield from 1.6 to 0.9 Ga. Contrib Mineral Petrol 150(2):174. https://doi.org/10.1007/s00410-005-0011-1

Tang J, Dietzel M, Böhm F, Köhler SJ, Eisenhauer A (2008) Sr2+/Ca2+ and 44Ca/40Ca fractionation during inorganic calcite formation: II. Ca isotopes. Geochim et Cosmochim Acta 72(15):3733–3745. https://doi.org/10.1016/j.gca.2008.05.033

Tillberg M, Drake H, Zack T, Kooijman E, Whitehouse MJ, Åström ME (2020) In situ Rb-Sr dating of slickenfibres in deep crystalline basement faults. Sci Rep 10(1):562. https://doi.org/10.1038/s41598-019-57262-5

Tillberg M, Drake H, Zack T, Hogmalm J, Kooijman E, Åström M (2021) Reconstructing craton-scale tectonic events via in situ Rb-Sr geochronology of poly-phased vein mineralization. Terra Nova 33(5):502–510. https://doi.org/10.1111/ter.12542

Torres RA, Choppin GR (1984) Europium (III) and Americium(III) stability constants with humic acid. Radiochim Acta 35(3):143–148. https://doi.org/10.1524/ract.1984.35.3.143

Tröjbom M, Söderbäck B (2006) Chemical characteristics of surface systems in the Forsmark area. Visualisation and statistical evaluation of data from shallow groundwater, precipitation, and regolith. Edited by Swedish Nuclear Fuel and Waste Management Co., Stockholm. Sweden (1402–3091). SKB Report R-06-19; IAEA Reference Number 37043709. http://inis.iaea.org/search/search.aspx?orig_q=RN:37043709

Tullborg E-L, Landström O, Wallin B (1999) Low-temperature trace element mobility influenced by microbial activity—indications from fracture calcite and pyrite in crystalline basement. Chem Geol 157(3):199–218. https://doi.org/10.1016/S0009-2541(99)00002-9

Tullborg E-L, Drake H, Sandström B (2008) Palaeohydrogeology: a methodology based on fracture mineral studies. Appl Geochem 23(7):1881–1897. https://doi.org/10.1016/j.apgeochem.2008.02.009

Viola G, Venvik Ganerød G, Wahlgren C-H (2009) Unraveling 1.5 Ga of brittle deformation history in the Laxemar-Simpevarp area, southeast Sweden: a contribution to the Swedish site investigation study for the disposal of highly radioactive nuclear waste. Tectonics. https://doi.org/10.1029/2009TC002461

Viola G (2008) Ductile and brittle structural evolution of the Laxemar-Simpevarp area: an independent analysis based on local and regional constraints. Edited by Swedish Nuclear Fuel and Waste Management Co., Stockholm. Sweden (1402–3091). SKB Report R-08-124; IAEA Reference Number 40012559. http://inis.iaea.org/search/search.aspx?orig_q=RN:40012559

Wahlgren C-H, Bergman T, Ahl M, Ekström M, Page L, Söderlund U (2007) Oskarshamn site investigation: modal and geochemical analyses of drill core samples 2007 and $_{40}$Ar/$_{39}$Ar dating of a dolerite. Classification of rock types in KLX15A, KLX16A, KLX19A, KLX20A and KLX21B. Oskarshamn site investigation. Edited by Swedish Nuclear Fuel and Waste Management Co., Stockholm. Sweden. SKB Report P-07-191. https://www.skb.com/publication/1570334/P-07-191.pdf

Wahlgren, Carl-Henric (2010) Oskarshamn site investigation bedrock geology - overview and excursion guide. Edited by Swedish Nuclear Fuel and Waste Management Co., Stockholm. Sweden (1402–3091). SKB Report R-10-05; IAEA Reference Number 41134045. http://inis.iaea.org/search/search.aspx?orig_q=RN:41134045

Wedepohl HK (1995) The composition of the continental crust. Geochim et Cosmochim Acta 59(7):1217–1232. https://doi.org/10.1016/0016-7037(95)00038-2

Withers SH, Peale RE, Schulte AF, Braunstein G, Beck KM, Hess WP, Reeder RJ (2003) Broad distribution of crystal-field environments for Nd^{3+} in calcite. Phys Chem Miner 30(7):440–448. https://doi.org/10.1007/s00269-003-0331-5

Xiong Y (2011) Organic species of Lanthanum in natural environments: Implications to mobility of rare earth elements in low temperature environments. Appl Geochem 26(7):1130–1137. https://doi.org/10.1016/j.apgeochem.2011.04.003

Zhong S, Mucci A (1989) Calcite and aragonite precipitation from seawater solutions of various salinities: precipitation rates and overgrowth compositions. Chem Geol 78(3):283–299. https://doi.org/10.1016/0009-2541(89)90064-8

Zhong S, Mucci A (1995) Partitioning of rare earth elements (REEs) between calcite and seawater solutions at 25°C and 1 atm, and high dissolved REE concentrations. Geochim et Cosmochim Acta 59(3):443–453. https://doi.org/10.1016/0016-7037(94)00381-U